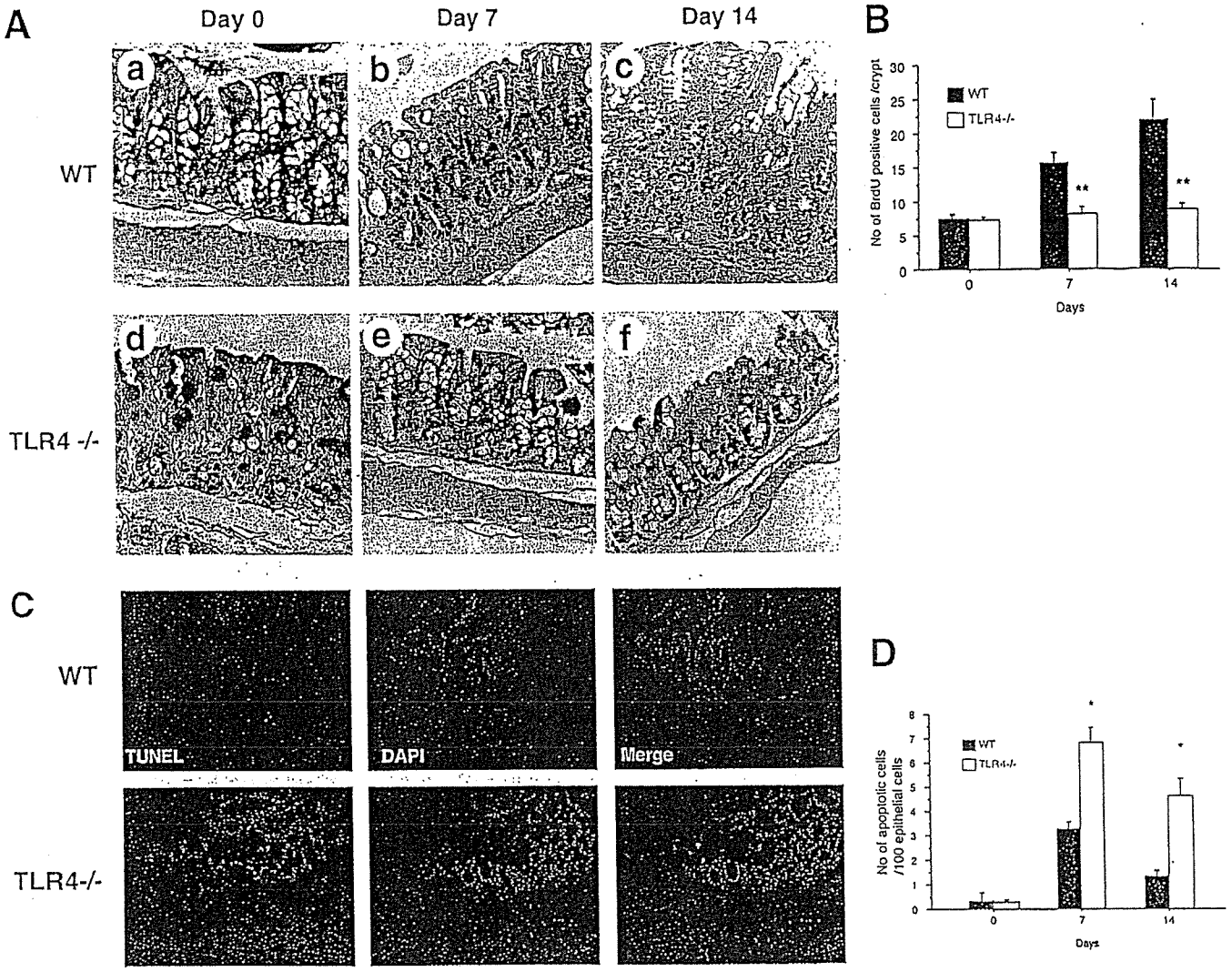

Figure 3. TLR4−/− mice have a persistent decrease in epithelial proliferation and increased apoptosis after 7 days of DSS treatment. (*A*) TLR4−/− and WT control mice were treated with 2.5% DSS for 7 days (*left panels*) followed by 7 days of recovery (*right panels*). Animals were injected with BrdU 90 minutes before death. Colonic sections taken from day 0 (*a*, WT; *d*, TLR4−/−), day 7 (*b*, WT; *e*, TLR4−/−), and day 14 (*c*, WT; *f*, TLR4−/−) were stained with anti-BrdU. BrdU-positive cells are identified by *black* staining of nuclei. TLR4−/− mice have fewer BrdU-positive cells in the crypts on (*e*) day 7 and on (*f*) day 14. Tissues were counterstained with methyl *green* (original magnification, 200×). (*B*) BrdU-positive cells were counted in 3 crypts of each colon segment per high-power field (9 crypts/mouse). *Bars* show the mean ± SEM of proliferating cells/crypts (n = 3 for each group on day 0 [ie, untreated], n = 5 for the other groups). The proliferating cells in TLR4−/− mice were significantly fewer than in WT controls after 7 days of DSS treatment (day 7) and during recovery (day 14) from DSS-induced colitis (**$P < .001$). (*C*) Apoptotic cells in the colonic crypt epithelial cells of TLR4−/− and WT controls were determined by TUNEL assay. Representative sections were taken on day 7 of DSS treatment. *Red* staining of nuclei indicates apoptotic cells, which was observed mainly in the surface epithelium. Sections were counterstained with 4′,6-diamidino-2-phenylindole (*blue*) to identify the orientation of nuclei. TLR4−/− mice showed increased apoptotic cells compared with WT controls (original magnification, 200×). (*D*) Numbers of apoptotic cells were counted in 300 total epithelial cells in 3 areas of each colon segment (n = 3 for each group on day 0 [untreated], n = 6–7 for the other groups). *Bars* show the mean ± SEM of the number of apoptotic cells per 100 total nuclei of the epithelial cells. There were significant increases of apoptotic cells in TLR4−/− mice compared with WT controls after 7 days of DSS treatment (*$P < .05$). The apoptotic cells were still increased in TLR4−/− mice even after recovery (day 14, *$P < .05$).

namely worse clinical signs of colitis and abnormal proliferation and apoptosis. To test this hypothesis, TLR4−/− mice were given PGE_2 by oral gavage twice a day concurrently with the DSS treatment period. These mice were compared with TLR4−/− mice and WT mice given DSS alone with PBS to control for the gavage solution. Compared with TLR4−/− PBS-treated mice, TLR4−/− mice treated with PGE_2 behaved similar to WT mice with respect to weight loss (Figure 4*A*) and rectal bleeding (Figure 4*B*). We next examined the effect of PGE_2 supplementation on proliferation and apoptosis. TLR4−/− mice given PGE_2 had significantly greater proliferation (Figure 4*C* and *D*) and reduced apoptosis (Figure 4*E* and *F*) than TLR4−/− mice given vehicle alone. Total histology scores were lower for PGE_2-treated TLR4−/− mice compared with control TLR4−/− mice because crypt damage was less (data not shown). PGE_2 treatment of wild-type DSS-treated mice showed no significant change in proliferation (WT cont, 14.5 ± 1.4; WT + PGE_2, 12.3 ± 1.6) and a small decrease in apoptosis (WT

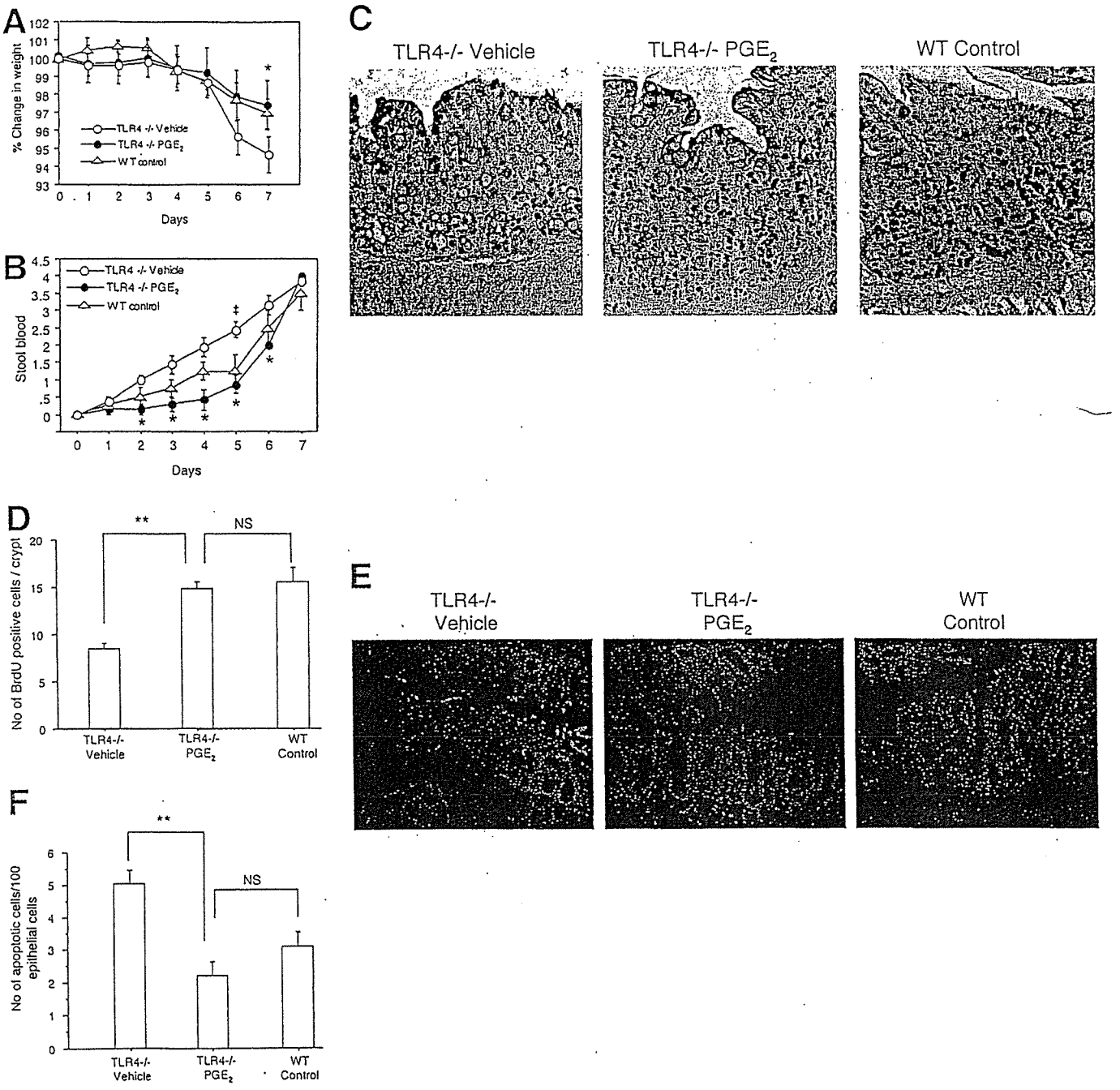

Figure 4. PGE_2 supplementation improves signs of colitis and restores epithelial healing after DSS-induced injury in TLR4−/− mice. (*A*) Weight change was examined daily during the 7 days of DSS treatment. Vehicle-treated (PBS) TLR4−/− mice had significantly more weight loss than WT control mice (*$P < .05$). PGE_2-treated TLR4−/− mice had significantly less weight loss than vehicle-treated TLR4−/− mice and are comparable with WT mice. The data represent the average (±SEM) of 3 independent experiments with a total of 19 mice (TLR4−/− vehicle [n = 6], TLR4−/− PGE_2 [n = 7], and WT controls [n = 6]). (*B*) PGE_2-treated TLR4−/− mice had a significant reduction in bleeding on days 2–6 compared with vehicle-treated (PBS) TLR4−/− mice (*$P < .05$). Stool blood was calculated as follows: 0 = no blood, 1 = trace occult blood positive, 2 = strongly occult blood positive, and 4 = bloody diarrhea. Standard error is shown. (*C*) BrdU labeling of intestinal epithelial cells was performed for vehicle-treated TLR4−/−, PGE_2-treated TLR4−/−, and WT controls at the end of 7 days of DSS treatment (original magnification, 200×). (*D*) BrdU-positive cells were counted per high-power field in 3 crypts of each colon segment (9 areas/mouse). *Bars* show the mean ± SEM of proliferating cells/crypts (n = 5 in each group). There is a significant increase in BrdU-positive cells in PGE_2-treated TLR4−/− mice compared with vehicle-treated TLR4−/− mice (**$P < .001$). PGE_2-treated TLR4−/− mice are not significantly different than WT mice. (*E*) Apoptotic cells in the crypt epithelial cells were determined by TUNEL assay. Representative sections were taken from vehicle-treated TLR4−/−, PGE_2-treated TLR4−/− mice, and WT controls as indicated. *Red* staining of nuclei indicates apoptotic cells. Sections were counterstained with 4′,6-diamidino-2-phenylindole (*blue*) to identify the nuclei of epithelial cells. PGE_2-treated TLR4−/− mice showed a marked decrease of apoptotic cells compared with vehicle-treated TLR−/− mice. The frequency of TUNEL-positive epithelial cells in PGE_2-treated TLR4−/− mice was similar to WT controls (original magnification, 200×). (*F*) Number of apoptotic cells was counted in 300 total epithelial cells in triplicate in 3 areas for each colon segment (n = 5 in each group). *Bars* show the mean ± SEM of the number of apoptotic cells per 100 total nuclei in the epithelial cells counted. There is a significant decrease of apoptotic cells in PGE_2-treated TLR4−/− mice compared with vehicle-treated TLR4−/− mice (**$P < .001$).

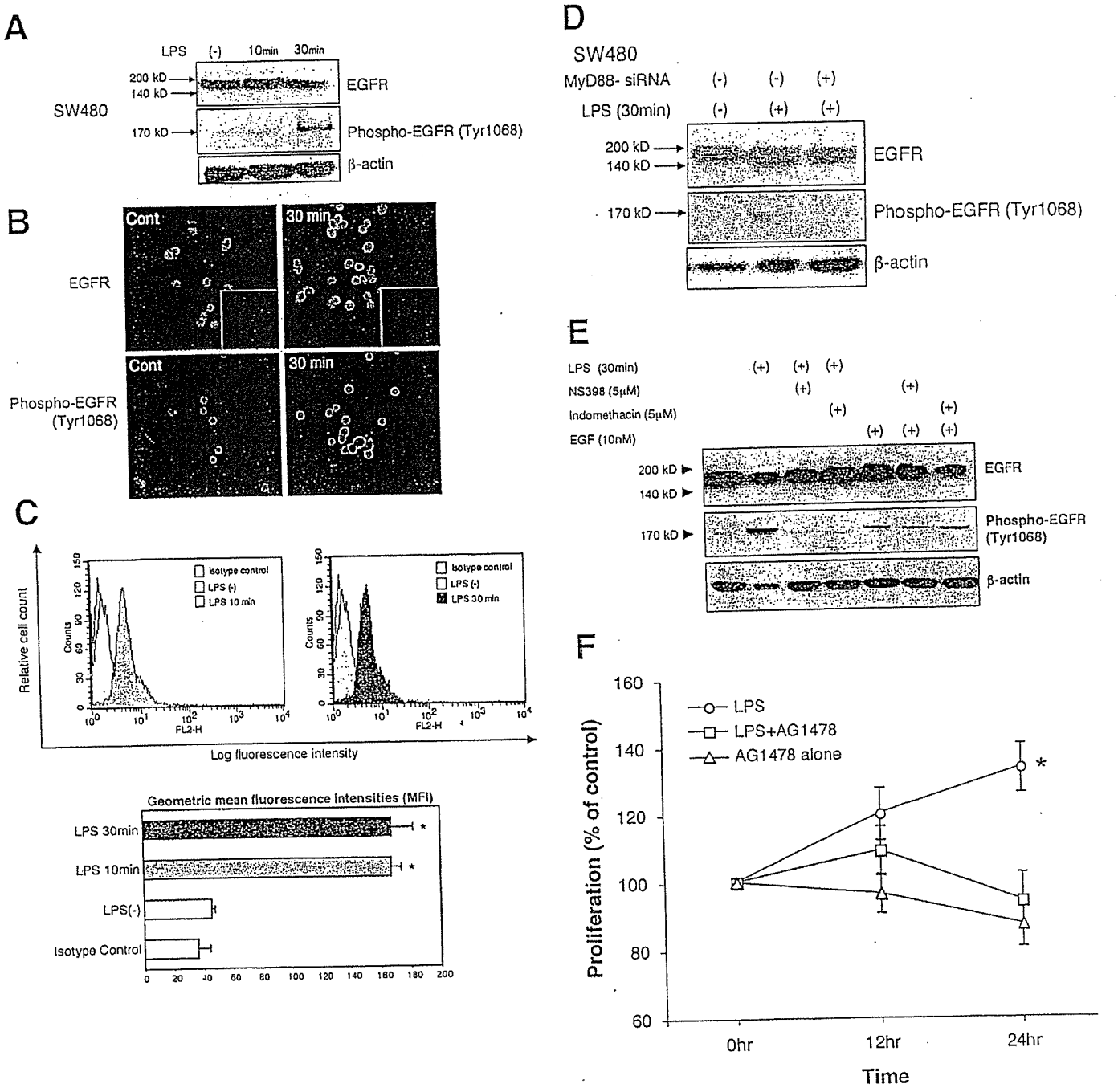

Figure 5. LPS induces EGFR phosphorylation in a MyD88-dependent fashion. (*A*) Western blot analysis of EGFR and its phosphorylation in human intestinal epithelial cell line SW480. Cells were stimulated with LPS for indicated periods. Blots of whole-cell lysates (25 μg/*lane*) were probed with either EGFR (*top panel*) or phosphorylated EGFR (*bottom panel*). LPS stimulated EGFR phosphorylation. Data are 1 representative experiment of 3 independent experiments with similar results. (*B*) Immunofluorescent staining for EGFR and phospho-EGFR in SW480. Cells were cultured on glass slides and treated with LPS (2 μg/mL) for indicated periods. Nuclei were stained with 4′,6-diamidino-2-phenylindole. After 30 minutes of stimulation, confocal images show an increased intensity of staining of phospho-EGFR but not EGFR. *Insets* show negative control in which primary antibodies were omitted. Original magnification, 400×. (*C*) Flow cytometric analysis of phospho-EGFR (Tyr1068) after stimulation with LPS for indicated periods of time. Histograms show an increase in log fluorescence intensity. *Bars* represent the geometric mean of fluorescence intensity of phospho-EGFR-positive cells ± SD based on 3 individual experiments (LPS, 2 μg/mL) with triplicate samples (*$P < .05$). (*D*) LPS-induced EGFR phosphorylation is MyD88 dependent. Western blot analysis of EGFR and its phosphorylated form are shown. Cells were stimulated with LPS for indicated periods. Blots of whole-cell lysates (25 μg/*lane*) were probed with EGFR or phospho-EGFR antibody. Cells transfected with MyD88 siRNA had no phosphorylation of EGFR in response to LPS. Data are 1 representative experiment of 3 independent experiments with similar results. (*E*) LPS-induced EGFR phosphorylation is Cox-2 dependent. Cells were stimulated with LPS (2 μg/mL) for 30 minutes with or without Cox inhibitors as indicated, and whole-cell lysates (22 μg/*lane*) were probed with EGFR or phospho-EGFR antibodies. Western blot analysis shows that EGFR phosphorylation is inhibited by a nonselective Cox-2 inhibitor, (NS398 5 μmol/L), or a Cox-1 and Cox-2 inhibitor (indomethacin selective, 5 μmol/L). As a control, EGF (10 nMol = 6 ng/mL) was added to cells for 30 minutes. EGF-mediated phosphorylation of the EGFR was not inhibited by Cox inhibitors (last 3 *lanes*). Data are 1 representative experiment of 5 independent experiments with similar results. (*F*) LPS induced cell proliferation via EGFR activation. SW480 cells were stimulated with LPS (2 μg/mL) for indicated periods with or without EGFR-specific tyrosine kinase inhibitor AG1478. Data are shown as the means ± SD of percentage of absorbance in comparison with nontreated control cells from 3 independent experiments.

cont, 3.1 ± 2; WT + PGE_2, 1.4 ± 1.3). These data suggest that PGE_2 is necessary and sufficient to restore epithelial healing as measured by proliferation and apoptosis in the injured intestinal epithelium.

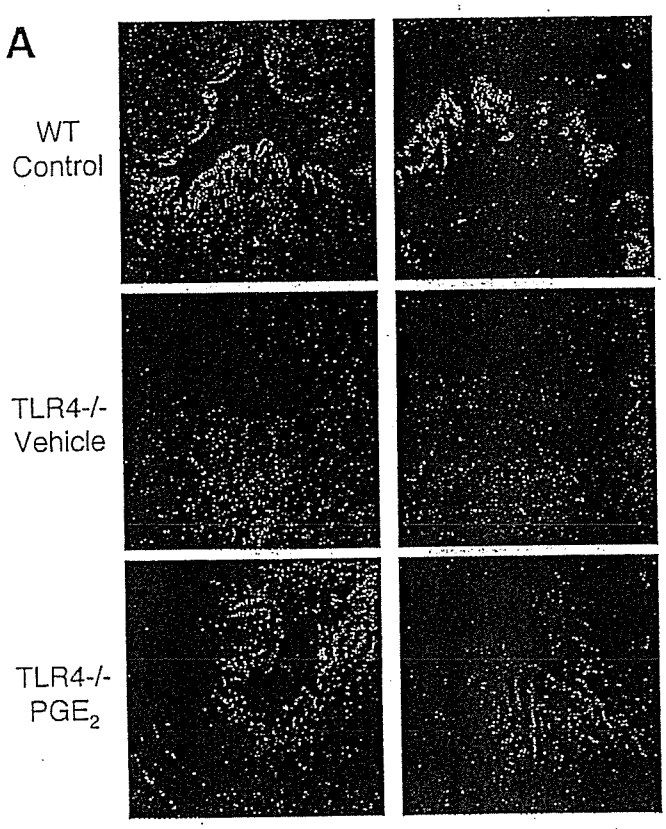

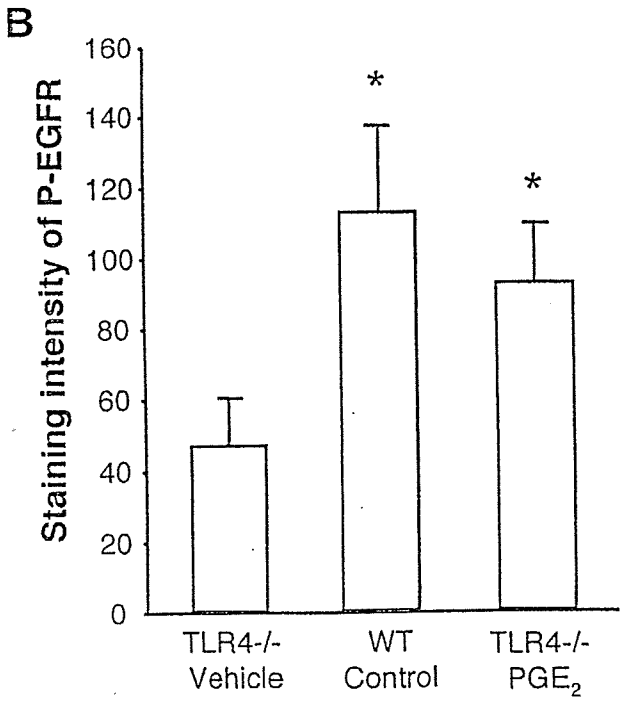

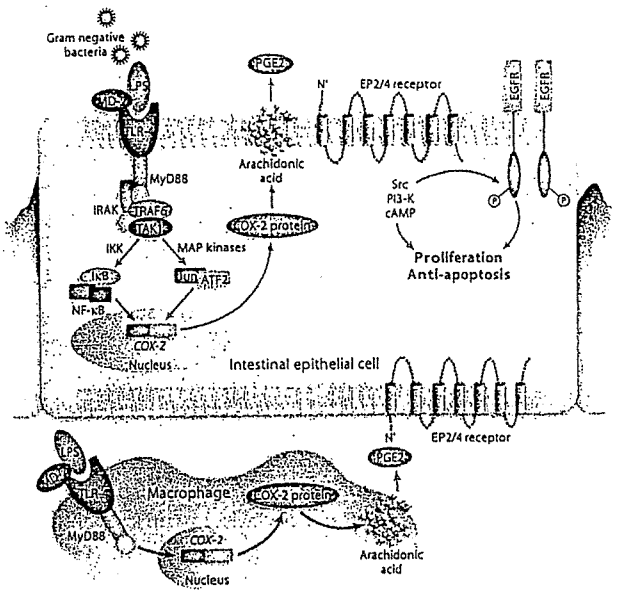

Figure 7. Model of TLR4-mediated Cox-2 regulation. In the setting of intestinal injury, LPS exposure of intestinal epithelial cells (possibly basolaterally) and lamina propria macrophages results in TLR4 activation and signaling via MyD88. This activates a variety of signaling pathways culminating in transcription factor translocation and engagement of the Cox-2 promoter. Cox-2 is transcribed and translated; it acts on arachidonic acid to generate PGG_2, which is converted rapidly to PGH_2 and then microsomal PGE synthase-1 converts it to PGE_2. PGE_2, through its receptors EP2 or EP4, can activate downstream signaling molecules such as the tyrosine kinase Src or the lipid kinase PI'3 kinase, which can lead to transactivation of EGFR. EGFR signaling is associated with proliferation and protection against apoptosis in intestinal epithelial cells. PGE_2 produced by macrophages also may act in *trans* on intestinal epithelial cells. In the absence of TLR4 signaling, Cox-2 expression is greatly decreased.

TLR4 Regulates Phosphorylation of the EGFR in Intestinal Epithelial Cells

Our data point to a link between TLR4-mediated induction of Cox-2 and PGE_2 production and intestinal injury. To understand the mechanism(s) by which PGE_2 mediates an effect on the intestinal epithelium, we examined the ability of LPS to stimulate EGFR phosphorylation. EGFR phosphorylation results in a variety of biologic events including induction of

Figure 6. TLR4−/− mice have decreased EGFR phosphorylation after DSS-induced colitis owing to defective production of mucosal PGE_2. (*A*) Immunofluorescent staining for phospho EGFR in the colon after 7 days of DSS treatment. Phosphorylated EGFR was strongly detected in surface epithelial cells in WT mice. PBS-treated TLR4−/− mice had decreased epithelial cell EGFR phosphorylation after DSS colitis. PGE_2 treatment partly restored the expression of phosphorylated EGFR. Two individual mouse tissue samples of each genotype with or without PGE_2 treatment are shown. (*B*) Quantification of the expression levels of phospho EGFR. Staining intensity of 10 randomly selected areas of epithelial cells per slide was analyzed using MetaMorph software. Staining intensity of phospho EGFR was decreased significantly in TLR4−/− mice compared with WT mice and PGE_2-treated TLR4−/− mice after 7 days of DSS treatment.

proliferation and protection against apoptosis.[43-46] PGE_2 mediates EGFR phosphorylation through induction of EGFR ligands or through intracellular mediators such as Src.[47,48] We hypothesized that LPS stimulation of intestinal epithelial cells would result in EGFR phosphorylation. SW480 cells were stimulated with LPS and total or phosphorylated EGFR was examined by Western blot and immunofluorescent staining (Figure 5*A* and *B*). LPS stimulated phosphorylation of EGFR. We further quantified LPS-induced EGFR phosphorylation by flow cytometric analysis (Figure 5*C*). LPS stimulation significantly increased EGFR phosphorylation. We then addressed whether this effect on EGFR was dependent on TLR-MyD88 signaling. EGFR phosphorylation was blocked by expression of MyD88 siRNA (Figure 5*D*) and partially by a specific inhibitor of Cox-2, NS398 (Figure 5*E*). EGF stimulation of SW480 cells resulted in EGFR phosphorylation that was not blocked by a Cox-2 inhibitor or indomethacin (Figure 5*E*). Because it also was possible that LPS-induced EGFR phosphorylation is upstream of Cox-2 expression, we used a specific EGFR tyrosine kinase inhibitor, AG1478, and asked whether inhibition blocked LPS-mediated induction of Cox-2 protein expression. Inhibiting EGFR tyrosine kinase activity had no effect on Cox-2 induction (data not shown). Finally, we asked whether inhibition of EGFR phosphorylation affected LPS-induced cell proliferation in SW480 cells. AG1478 blocked LPS-induced cell proliferation (Figure 5*F*). These data suggest that TLR4-mediated induction of PGE_2 production may stimulate epithelial proliferation by an EGFR-dependent mechanism.

Given the results of TLR4-regulating phosphorylation of EGFR in vitro, we hypothesized that TLR4−/− mice have decreased phosphorylation of EGFR in intestinal epithelial cells in vivo. To test this hypothesis, we used immunohistochemistry to evaluate the expression of phosphorylated EGFR in intestinal epithelial cells after DSS-induced colitis. WT mice had significantly higher expression of phosphorylated EGFR in intestinal epithelial cells than TLR4−/− mice after DSS-induced colitis (Figure 6*A*). TLR4−/− mice given PGE_2 treatment had restored expression of phosphorylated EGFR to nearly WT levels (Figure 6*A*). Omission of primary antibody did not show any staining (data not shown). Computer analysis using the MetaMorph program was used to quantify intensity of staining in the intestinal epithelium (Figure 6*B*). We conclude from these results that impaired epithelial repair seen in TLR4−/− mice is at least partly owing to impaired activation of epithelial cell EGFR, which in turn may be owing to decreased mucosal production of PGE_2 in response to inflammation.

Discussion

In this study, we show a requirement for TLR4 in regulating Cox-2 expression in both intestinal epithelial cells and lamina propria macrophages. In our model (Figure 7), epithelial injury permits exposure of intestinal epithelial cells and lamina propria macrophages to gram-negative bacteria and LPS. TLR4 signaling via MyD88 activates a signaling cascade that results in enhanced transcription of *Cox-2* and increased production of PGE_2. The clinical manifestations of increased rectal bleeding seen in TLR4[3] mice likely are caused by the epithelial defect in proliferation and apoptosis because correcting the defect with native exogenous PGE_2 restored mice to WT levels of rectal bleeding. These data suggest that a relative deficiency in PGE_2 production is likely to play an important role in the observed TLR4[3] phenotype. Our in vitro data support the idea that the effect of TLR4 on Cox-2 expression and other downstream mediators of epithelial repair can occur directly by LPS signaling in intestinal epithelial cells. In vivo, however, there is likely to be a contribution by lamina propria macrophages acting in *trans* on the epithelium by way of contact or secreted factors including PGE_2.

We present data that the colonic epithelium depends on bacterial-derived signals to activate the complex program involved in tissue repair. With the discovery of TLR molecules, the exact pathways by which this occurs may be better understood. The notion that TLR signaling is relevant and necessary for repair of injury is exemplified in a recent study showing that mice deficient in MyD88 or TLR4/TLR2 signaling were impaired in their ability to heal after acute lung injury.[49] The authors describe that extracellular matrix hyaluronan, either directly or indirectly, activates TLR2 and TLR4 signaling, resulting in inflammatory cell transmigration and protection against apoptosis. In the absence of TLR signaling there is decreased inflammatory infiltrate in the lungs of mice, but paradoxically animals have decreased survival. The similarities of our results in a model of intestinal epithelial cell injury suggest a common theme of repair linked to an inflammatory signal.

To understand what role TLR4 might be playing in the setting of DSS-induced injury we examined the literature for known effects of LPS on the intestinal epithelium. Investigators have shown that LPS can induce proliferation of intestinal epithelial cell (IEC)-6 cells in culture through a tumor necrosis factor–dependent mechanism.[50] Grishin et al[51,52] recently showed that LPS stimulates Cox-2 in a rat intestinal epithelial cell line and have focused on the role this may play in necrotizing enterocolitis. Although our study is not the first to show a link between LPS and Cox-2, we believe our studies show the degree to which TLR4 is required for intestinal expression of Cox-2 in vivo and the dependence of TLR4-mediated Cox-2 expression in repair of the damaged epithelium. Rakoff-Nahoum et al[14] examined proliferation in MyD88−/− mice in the setting of radiation injury and found a decrease in proliferative response but did not investigate the underlying mechanism in detail. Finally, Pull et al[3] used a bone-marrow chimera model to look at the relative contribution of MyD88 expression in immune vs nonimmune cells in the colonic proliferative response after DSS colitis. They describe a prominent role for MyD88-expressing lamina propria mesenchymal cells in the proliferative response of the epithelium in DSS-treated mice. Interestingly, in supplemental material accompanying the article by Pull et al,[3] Cox-2 was expressed highly in mesenchyme derived from conventionalized RAG1−/− mouse intestine compared with MyD88−/− mice, suggesting that the Cox-2 from mesenchymal cells may play a role in epithelial repair. Given the broad nature of the defect in TLR, interleukin-1, and interleukin-18 signaling in MyD88−/− cells, the prior studies do not address the specific contribution of TLR4 signaling nor the mechanisms underlying the proliferative defect.

Other studies were performed before the identification of TLR4 as the receptor for LPS. Studies in C3H/HeJ mice with a mutation in TLR4[8] found that crypt epithelial proliferation was decreased after DSS and could be restored by PGE_2.[53] Similar to Wang et al,[54] we used native PGE_2 administered orally rather than the longer-acting dimethyl-PGE_2. We used oral PGE_2 be-

cause of previous evidence that this approach led to increased levels of PGE_2 in the blood and intestine and altered colon physiology. Riehl et al[21] described that systemic LPS protected against radiation-induced epithelial apoptosis in intestinal crypts through a mechanism that depends on PGE_2 production.

The link between Cox-2 and PGE_2 in protection from colitis is highlighted in a variety of studies. Cox-2−/− mice show increased susceptibility to DSS-induced colitis, which correlates with their inability to produce PGE_2.[22] Animals deficient in the PGE_2 receptor, EP4, are more susceptible to DSS injury.[55] Several mechanisms underlie the protective effects of PGE_2. PGE_2, through its receptors EP2 or EP4, may stimulate EGFR phosphorylation through intracellular kinases such as Src or by increased expression of amphiregulin, an EGFR ligand.[46-48,56] PGE_2 protects against radiation-induced intestinal epithelial cell apoptosis through an EGFR and Akt-dependent effect on Bax.[48] Signaling downstream of EGFR is involved in growth, repair, and barrier integrity of the gastrointestinal mucosa.[57-59] Increased susceptibility of EGFR-deficient mice to DSS-induced colitis also has been reported.[60]

Studies also have shown that Cox-2 levels[41] and PGE_2 production[61-63] are increased in inflammatory bowel disease. Cox-2 overexpression characterizes dysplasia and colon cancer.[64-66] Recent work shows that PGE_2-dependent colon carcinogenesis involves deregulated phosphoinositide 3 (PI-3) kinase signaling and increased expression of β-catenin.[67] An increase in EGFR phosphorylation has been described in the mucosa of patients with ulcerative colitis.[68] This model is consistent with the known benefit of Cox-2 inhibitors and EGFR antagonists such as cetuximab in the prevention or treatment of colon cancer. In IBD, it remains controversial whether Cox-2 inhibitors worsen symptoms of the disease.[69] Short-term studies have shown that Cox-2 inhibitors do not flare colitis,[70] but long-term use, as would be required for chemoprevention, might flare disease. Mesalamines inhibit arachidonic acid metabolism to PGE_2 and have a modest chemopreventive benefit in patients with ulcerative colitis,[71] whereas other immunomodulators such as 6-mercaptopurine do not.[72] These data suggest an inflammation-independent effect of mesalamines, possibly through inhibition of PGE_2.

Our studies highlight the previous unknown dependence of Cox-2 expression by TLR4 in the intestine. In the acute response to injury, TLR4 signaling results in increased Cox-2 and PGE_2 production, which is beneficial. We may speculate that long-term, persistent TLR4 signaling may contribute to colitis-associated cancers. Strategies aimed at dampening TLR4 signaling may reduce chronic inflammation and the drive toward carcinogenesis.

References

1. Hooper LV, Stappenbeck TS, Hong CV, Gordon JI. Angiogenins: a new class of microbicidal proteins involved in innate immunity. Nat Immunol 2003;4:269–273.
2. Abrams GD, Bauer H, Sprinz H. Influence of the normal flora on mucosal morphology and cellular renewal in the ileum. A comparison of germ-free and conventional mice. Lab Invest 1963;12: 355–364.
3. Pull SL, Doherty JM, Mills JC, Gordon JI, Stappenbeck TS. Activated macrophages are an adaptive element of the colonic epithelial progenitor niche necessary for regenerative responses to injury. Proc Natl Acad Sci U S A 2005;102:99–104.
4. Kitajima S, Morimoto M, Sagara E, Shimizu C, Ikeda Y. Dextran sodium sulfate-induced colitis in germ-free IQI/Jic mice. Exp Anim 2001;50:387–395.
5. Sartor RB. Clinical applications of advances in the genetics of IBD. Rev Gastroenterol Disord 2003;3:S9–S17.
6. Kim SC, Tonkonogy SL, Albright CA, Tsang J, Balish EJ, Braun J, Huycke MM, Sartor RB. Variable phenotypes of enterocolitis in interleukin 10-deficient mice monoassociated with two different commensal bacteria. Gastroenterology 2005;128:891–906.
7. Pasare C, Medzhitov R. Toll-like receptors: linking innate and adaptive immunity. Adv Exp Med Biol 2005;560:11–18.
8. Poltorak A, He X, Smirnova I, Liu MY, Huffel CV, Du X, Birdwell D, Alejos E, Silva M, Galanos C, Freudenberg M, Ricciardi-Castagnoli P, Layton B, Beutler B. Defective LPS signaling in C3H/HeJ and C57BL/10ScCr mice: mutations in Tlr4 gene. Science 1998;282: 2085–2088.
9. Hoshino K, Takeuchi O, Kawai T, Sanjo H, Ogawa T, Takeda Y, Takeda K, Akira S. Cutting edge: Toll-like receptor 4 (TLR4)-deficient mice are hyporesponsive to lipopolysaccharide: evidence for TLR4 as the Lps gene product. J Immunol 1999;162: 3749–3752.
10. Travassos LH, Girardin SE, Philpott DJ, Blanot D, Nahori MA, Werts C, Boneca IG. Toll-like receptor 2-dependent bacterial sensing does not occur via peptidoglycan recognition. EMBO Rep 2004;5:1000–1006.
11. Sato S, Sanjo H, Takeda K, Ninomiya-Tsuji J, Yamamoto M, Kawai T, Matsumoto K, Takeuchi O, Akira S. Essential function for the kinase TAK1 in innate and adaptive immune responses. Nat Immunol 2005;6:1087–1095.
12. Cario E, Gerken G, Podolsky DK. Toll-like receptor 2 enhances ZO-1-associated intestinal epithelial barrier integrity via protein kinase C. Gastroenterology 2004;127:224–238.
13. Vora P, Youdim A, Thomas LS, Fukata M, Tesfay SY, Lukasek K, Michelsen KS, Wada A, Hirayama T, Arditi M, Abreu MT. Beta-defensin-2 expression is regulated by TLR signaling in intestinal epithelial cells. J Immunol 2004;173:5398–5405.
14. Rakoff-Nahoum S, Paglino J, Eslami-Varzaneh F, Edberg S, Medzhitov R. Recognition of commensal microflora by Toll-like receptors is required for intestinal homeostasis. Cell 2004;118: 229–241.
15. Fukata M, Michelsen KS, Eri R, Thomas LS, Hu B, Lukasek K, Nast CC, Lechago J, Xu R, Naiki Y, Soliman A, Arditi M, Abreu MT. Toll-like receptor-4 is required for intestinal response to epithelial injury and limiting bacterial translocation in a murine model of acute colitis. Am J Physiol 2005;288:G1055–G1065.
16. Araki A, Kanai T, Ishikura T, Makita S, Uraushihara K, Iiyama R, Totsuka T, Takeda K, Akira S, Watanabe M. MyD88-deficient mice develop severe intestinal inflammation in dextran sodium sulfate colitis. J Gastroenterol 2005;40:16–23.
17. Backlund MG, Mann JR, Holla VR, Buchanan FG, Tai HH, Musiek ES, Milne GL, Katkuri S, DuBois RN. 15-Hydroxyprostaglandin dehydrogenase is down-regulated in colorectal cancer. J Biol Chem 2005;280:3217–3223.
18. Subbaramaiah K, Yoshimatsu K, Scherl E, Das KM, Glazier KD, Golijanin D, Soslow RA, Tanabe T, Naraba H, Dannenberg AJ. Microsomal prostaglandin E synthase-1 is overexpressed in inflammatory bowel disease. Evidence for involvement of the transcription factor Egr-1. J Biol Chem 2004;279:12647–12658.
19. Otani T, Yamaguchi K, Scherl E, Du B, Tai HH, Greifer M, Petrovic L, Daikoku T, Dey SK, Subbaramaiah K, Dannenberg AJ. Levels of NAD(+)-dependent 15-hydroxyprostaglandin dehydrogenase are reduced in inflammatory bowel disease: evidence for involvement of TNF-alpha. Am J Physiol 2006;290:G361–G368.
20. Newberry RD, McDonough JS, Stenson WF, Lorenz RG. Spontaneous and continuous cyclooxygenase-2-dependent prostaglandin E2 production by stromal cells in the murine small intestine

lamina propria: directing the tone of the intestinal immune response. J Immunol 2001;166:4465–4472.
21. Riehl T, Cohn S, Tessner T, Schloemann S, Stenson WF. Lipopolysaccharide is radioprotective in the mouse intestine through a prostaglandin-mediated mechanism. Gastroenterology 2000; 118:1106–1116.
22. Morteau O, Morham SG, Sellon R, Dieléman LA, Langenbach R, Smithies O, Sartor RB. Impaired mucosal defense to acute colonic injury in mice lacking cyclooxygenase-1 or cyclooxygenase-2. J Clin Invest 2000;105:469–478.
23. Wang D, Buchanan FG, Wang H, Dey SK, DuBois RN. Prostaglandin E2 enhances intestinal adenoma growth via activation of the Ras-mitogen-activated protein kinase cascade. Cancer Res 2005;65:1822–1829.
24. Holla VR, Wang D, Brown JR, Mann JR, Katkuri S, DuBois RN. Prostaglandin E2 regulates the complement inhibitor CD55/decay-accelerating factor in colorectal cancer. J Biol Chem 2005; 280:476–483.
25. Atreya R, Mudter J, Finotto S, Mullberg J, Jostock T, Wirtz S, Schutz M, Bartsch B, Holtmann M, Becker C, Strand D, Czaja J, Schlaak JF, Lehr HA, Autschbach F, Schurmann G, Nishimoto N, Yoshizaki K, Ito H, Kishimoto T, Galle PR, Rose-John S, Neurath MF. Blockade of interleukin 6 trans signaling suppresses T-cell resistance against apoptosis in chronic intestinal inflammation: evidence in Crohn disease and experimental colitis in vivo. Nat Med 2000;6:583–588.
26. Cooper HS, Murthy SN, Shah RS, Sedergran DJ. Clinicopathologic study of dextran sulfate sodium experimental murine colitis. Lab Invest 1993;69:238–249.
27. Siegmund B, Lehr HA, Fantuzzi G. Leptin: a pivotal mediator of intestinal inflammation in mice. Gastroenterology 2002;122:2011–2025.
28. Moss SF, Holt PR. Apoptosis in the intestine. Gastroenterology 1996;111:567–568.
29. Inoue H, Nanayama T, Hara S, Yokoyama C, Tanabe T. The cyclic AMP response element plays an essential role in the expression of the human prostaglandin-endoperoxide synthase 2 gene in differentiated U937 monocytic cells. FEBS Lett 1994;350:51–54.
30. Inoue H, Yokoyama C, Hara S, Tone Y, Tanabe T. Transcriptional regulation of human prostaglandin-endoperoxide synthase-2 gene by lipopolysaccharide and phorbol ester in vascular endothelial cells. Involvement of both nuclear factor for interleukin-6 expression site and cAMP response element. J Biol Chem 1995; 270:24965–24971.
31. Mukherji M. Phosphoproteomics in analyzing signaling pathways. Expert Rev Proteomics 2005;2:117–128.
32. Irish JM, Hovland R, Krutzik PO, Perez OD, Bruserud O, Gjertsen BT, Nolan GP. Single cell profiling of potentiated phospho-protein networks in cancer cells. Cell 2004;118:217–228.
33. Rhee SH, Hwang D. Murine Toll-like receptor 4 confers lipopolysaccharide responsiveness as determined by activation of NF kappa B and expression of the inducible cyclooxygenase. J Biol Chem 2000;275:34035–34040.
34. Suzuki M, Hisamatsu T, Podolsky DK. Gamma interferon augments the intracellular pathway for lipopolysaccharide (LPS) recognition in human intestinal epithelial cells through coordinated up-regulation of LPS uptake and expression of the intracellular Toll-like receptor 4-MD-2 complex. Infect Immun 2003;71:3503–3511.
35. Yoshimatsu K, Golijanin D, Paty PB, Soslow RA, Jakobsson PJ, DeLellis RA, Subbaramaiah K, Dannenberg AJ. Inducible microsomal prostaglandin E synthase is overexpressed in colorectal adenomas and cancer. Clin Cancer Res 2001;7:3971–3976.
36. Backlund MG, Mann JR, Dubois RN. Mechanisms for the prevention of gastrointestinal cancer: the role of prostaglandin E2. Oncology 2005;69(Suppl 1):28–32.
37. Meyer TA, Noguchi Y, Ogle CK, Tiao G, Wang JJ, Fischer JE, Hasselgren PO. Endotoxin stimulates interleukin-6 production in intestinal epithelial cells. A synergistic effect with prostaglandin E2. Arch Surg 1994;129:1290–1295.
38. Longo WE, Damore LJ, Mazuski JE, Smith GS, Panesar N, Kaminski DL. The role of cyclooxygenase-1 and cyclooxygenase-2 in lipopolysaccharide and interleukin-1 stimulated enterocyte prostanoid formation. Mediators Inflamm 1998;7:85–91.
39. Grossman EM, Longo WE, Mazuski JE, Panesar N, Kaminski DL. Role of cytoplasmic and secretory phospholipase A2 in intestinal epithelial cell prostaglandin E2 formation. Int J Surg Investig 2000;1:467–476.
40. Newberry RD, McDonough JS, Stenson WF, Lorenz RG. Spontaneous and continuous cyclooxygenase-2-dependent prostaglandin E2 production by stromal cells in the murine small intestine lamina propria: directing the tone of the intestinal immune response. J Immunol 2001;166:4465–4472.
41. Singer II, Kawka DW, Schloemann S, Tessner T, Riehl T, Stenson WF. Cyclooxygenase 2 is induced in colonic epithelial cells in inflammatory bowel disease. Gastroenterology 1998;115:297–306.
42. Watson AJ, Chu S, Sieck L, Gerasimenko O, Bullen T, Campbell F, McKenna M, Rose T, Montrose MH. Epithelial barrier function in vivo is sustained despite gaps in epithelial layers. Gastroenterology 2005;129:902–912.
43. Stern LE, Erwin CR, O'Brien DP, Huang F, Warner BW. Epidermal growth factor is critical for intestinal adaptation following small bowel resection. Microsc Res Tech 2000;51:138–148.
44. Podolsky DK. Mechanisms of regulatory peptide action in the gastrointestinal tract: trefoil peptides. J Gastroenterol 2000; 35(Suppl 12):69–74.
45. Wu R, Abramson AL, Shikowitz MJ, Dannenberg AJ, Steinberg BM. Epidermal growth factor-induced cyclooxygenase-2 expression is mediated through phosphatidylinositol-3 kinase, not mitogen-activated protein/extracellular signal-regulated kinase kinase, in recurrent respiratory papillomas. Clin Cancer Res 2005; 11:6155–6161.
46. Dannenberg AJ, Lippman SM, Mann JR, Subbaramaiah K, DuBois RN. Cyclooxygenase-2 and epidermal growth factor receptor: pharmacologic targets for chemoprevention. J Clin Oncol 2005; 23:254–266.
47. Pai R, Soreghan B, Szabo IL, Pavelka M, Baatar D, Tarnawski AS. Prostaglandin E2 transactivates EGF receptor: a novel mechanism for promoting colon cancer growth and gastrointestinal hypertrophy. Nat Med 2002;8:289–293.
48. Tessner TG, Muhale F, Riehl TE, Anant S, Stenson WF. Prostaglandin E2 reduces radiation-induced epithelial apoptosis through a mechanism involving AKT activation and bax translocation. J Clin Invest 2004;114:1676–1685.
49. Jiang D, Liang J, Fan J, Yu S, Chen S, Luo Y, Prestwich GD, Mascarenhas MM, Garg HG, Quinn DA, Homer RJ, Goldstein DR, Bucala R, Lee PJ, Medzhitov R, Noble PW. Regulation of lung injury and repair by Toll-like receptors and hyaluronan. Nat Med 2005;11:1173–1179.
50. Ruemmele FM, Beaulieu JF, Dionne S, Levy E, Seidman EG, Cerf-Bensussan N, Lentze MJ. Lipopolysaccharide modulation of normal enterocyte turnover by Toll-like receptors is mediated by endogenously produced tumour necrosis factor alpha. Gut 2002; 51:842–848.
51. Grishin AV, Wang J, Hackam DJ, Qureshi F, Upperman JS, Zamora R, Ford HR. p38 MAP kinase mediates endotoxin-induced expression of cyclooxygenase-2 in enterocytes. Surgery 2004;136: 329–335.
52. Grishin AV, Wang J, Potoka DA, Hackam DJ, Upperman JS, Boyle P, Zamora R, Ford HR. Lipopolysaccharide induces cyclooxygenase-2 in intestinal epithelium via a noncanonical p38 MAPK pathway. J Immunol 2006;176:580–588.

53. Tessner TG, Cohn SM, Schloemann S, Stenson WF. Prostaglandins prevent decreased epithelial cell proliferation associated with dextran sodium sulfate injury in mice. Gastroenterology 1998;115:874–882.
54. Wang D, Wang H, Shi Q, Katkuri S, Walhi W, Desvergne B, Das SK, Dey SK, DuBois RN. Prostaglandin E(2) promotes colorectal adenoma growth via transactivation of the nuclear peroxisome proliferator-activated receptor delta. Cancer Cell 2004;6:285–295.
55. Kabashima K, Saji T, Murata T, Nagamachi M, Matsuoka T, Segi E, Tsuboi K, Sugimoto Y, Kobayashi T, Miyachi Y, Ichikawa A, Narumiya S. The prostaglandin receptor EP4 suppresses colitis, mucosal damage and CD4 cell activation in the gut. J Clin Invest 2002;109:883–893.
56. Buchanan FG, Wang D, Bargiacchi F, DuBois RN. Prostaglandin E2 regulates cell migration via the intracellular activation of the epidermal growth factor receptor. J Biol Chem 2003;278:35451–35457.
57. Konturek PK, Brzozowski T, Konturek SJ, Dembinski A. Role of epidermal growth factor, prostaglandin, and sulfhydryls in stress-induced gastric lesions. Gastroenterology 1990;99:1607–1615.
58. Romano M, Polk WH, Awad JA, Arteaga CL, Nanney LB, Wargovich MJ, Kraus ER, Boland CR, Coffey RJ. Transforming growth factor alpha protection against drug-induced injury to the rat gastric mucosa in vivo. J Clin Invest 1992;90:2409–2421.
59. Playford RJ, Wright NA. Why is epidermal growth factor present in the gut lumen? Gut 1996;38:303–305.
60. Egger B, Buchler MW, Lakshmanan J, Moore P, Eysselein VE. Mice harboring a defective epidermal growth factor receptor (waved-2) have an increased susceptibility to acute dextran sulfate-induced colitis. Scand J Gastroenterol 2000;35:1181–1187.
61. Carty E, De Brabander M, Feakins RM, Rampton DS. Measurement of in vivo rectal mucosal cytokine and eicosanoid production in ulcerative colitis using filter paper. Gut 2000;46:487–492.
62. Sharon P, Ligumsky M, Rachmilewitz D, Zor U. Role of prostaglandins in ulcerative colitis. Enhanced production during active disease and inhibition by sulfasalazine. Gastroenterology 1978; 75:638–640.
63. Wiercinska-Drapalo A, Flisiak R, Prokopowicz D. Effects of ulcerative colitis activity on plasma and mucosal prostaglandin E2 concentration. Prostaglandins Other Lipid Mediat 1999;58:159–165.
64. Sheehan KM, O'Connell F, O'Grady A, Conroy RM, Leader MB, Byrne MF, Murray FE, Kay EW. The relationship between cyclooxygenase-2 expression and characteristics of malignant transformation in human colorectal adenomas. Eur J Gastroenterol Hepatol 2004;16:619–625.
65. Konturek PC, Kania J, Burnat G, Hahn EG, Konturek SJ. Prostaglandins as mediators of COX-2 derived carcinogenesis in gastrointestinal tract. J Physiol Pharmacol 2005;56(Suppl 5):57–73.
66. Wang D, Mann JR, DuBois RN. The role of prostaglandins and other eicosanoids in the gastrointestinal tract. Gastroenterology 2005;128:1445–1461.
67. Castellone MD, Teramoto H, Williams BO, Druey KM, Gutkind JS. Prostaglandin E2 promotes colon cancer cell growth through a Gs-axin-beta-catenin signaling axis. Science 2005;310:1504–1510.
68. Malecka-Panas E, Kordek R, Biernat W, Tureaud J, Liberski PP, Majumdar AP. Differential activation of total and EGF receptor (EGF-R) tyrosine kinase (tyr-k) in the rectal mucosa in patients with adenomatous polyps, ulcerative colitis and colon cancer. Hepatogastroenterology 1997;44:435–440.
69. Matuk R, Crawford J, Abreu MT, Targan SR, Vasiliauskas EA, Papadakis KA. The spectrum of gastrointestinal toxicity and effect on disease activity of selective cyclooxygenase-2 inhibitors in patients with inflammatory bowel disease. Inflamm Bowel Dis 2004;10:352–356.
70. Sandborn W, Stenson W, Brynskov J, Steidle G, Robbins J. Safety of celecoxib in patients with ulcerative colitis in remission: a randomized, double-blind, placebo-controlled study. Clin Gastroenterol Hepatol 2006;4:157–159.
71. Velayos FS, Terdiman JP, Walsh JM. Effect of 5-aminosalicylate use on colorectal cancer and dysplasia risk: a systematic review and metaanalysis of observational studies. Am J Gastroenterol 2005;100:1345–1353.
72. Matula S, Croog V, Itzkowitz S, Harpaz N, Bodian C, Hossain S, Ullman T. Chemoprevention of colorectal neoplasia in ulcerative colitis: the effect of 6-mercaptopurine. Clin Gastroenterol Hepatol 2005;3:1015–1021.

Received January 9, 2006. Accepted June 2, 2006.

Address requests for reprints to: Dr Maria T. Abreu, Division of Gastroenterology, Inflammatory Bowel Disease Center, Mt. Sinai School of Medicine, 1425 Madison Avenue, 11-23D, New York, New York 10029. e-mail: maria.abreau@mssm.edu; fax: (212) 659-9853.

Supported by National Institutes of Health grants AI052266 and DK069594 (M.T.A.), the New York Crohn's Foundation (A.J.D.), and a Uehara Memorial Foundation Research Fellowship (M.F.).

Dimerization Is Crucial for the Function of the Na^+/H^+ Exchanger NHE1[†]

Takashi Hisamitsu, Youssef Ben Ammar, Tomoe Y. Nakamura, and Shigeo Wakabayashi*

Department of Molecular Physiology, National Cardiovascular Center Research Institute, Suita, Osaka 565-8565, Japan

Received May 2, 2006; Revised Manuscript Received August 15, 2006

ABSTRACT: The Na^+/H^+ exchanger 1 (NHE1) exists as a homo-dimer in the plasma membranes. In the present study, we have investigated the functional significance of the dimerization, using two nonfunctional NHE1 mutants, surface-expression-deficient G309V and transport-deficient E262I. Biochemical and immunocytochemical experiments revealed that these NHE1 mutants are capable of interacting with the wild-type NHE1 and, thus, forming a heterodimer. Expression of G309V retained the wild-type NHE1 to the ER membranes, suggesting that NHE1 would first form a dimer in the ER. On the other hand, expression of E262I markedly reduced the exchange activity of the wild-type NHE1 through an acidic shift in the intracellular pH (pH_i) dependence, suggesting that dimerization is required for exchange activity in the physiological pH_i range. However, a dominant−negative effect of E262I was not detected when exchange activity was measured at acidic pH_i, implying that one active subunit is sufficient to catalyze ion transport when the intracellular H^+ concentration is sufficiently high. Furthermore, intermolecular cysteine cross-linking at extracellular position Ser^{375} with a bifunctional sulfhydryl reagent dramatically inhibited exchange activity mainly by inducing the acidic shift of pH_i dependence and abolished extracellular stimuli-induced activation of NHE1 without causing a large change in the affinities for extracellular Na^+ or an inhibitor EIPA. Because monofunctional sulfhydryl regents had no effect, it is likely that cross-linking inhibited the activity of NHE1 by restricting a coupled motion between the two subunits during transport. Taken together, these data support the view that dimerization of two active subunits are required for NHE1 to possess the exchange activity in the neutral pH_i range, although each subunit is capable of catalyzing transport in the acidic pH_i range.

The Na^+/H^+ exchanger (NHE[1]) is a member of the secondary active transporter family, which catalyzes the exchange of Na^+ for H^+ (*1*−*5*). NHE isoforms (NHE1−NHE9) possess a common structural feature, that is, the molecules have two large functional domains, an amino (*N*-) terminal membrane domain consisting of multiple membrane-spanning helices and a long carboxyl (*C*-) terminal hydrophilic domain. Of nine known isoforms, NHE1 is ubiquitously expressed and is responsible for the control of intracellular pH (pH_i) and cell volume (*1*−*5*). NHE1 is known to be activated in response to various extrinsic stimuli such as hormones, growth factors, and changes in the medium osmolarity, presumably through the interaction of various signaling molecules with the *C*-terminal cytoplasmic domain. Importantly, such activation of NHE1 is thought to be exerted through a conformational change of the exchanger molecule, which is triggered by protonation at a H^+-modifier or pH sensor site that is distinct from the H^+-transport site (*6*−*8*).

In contrast to the extensive studies investigating the regulatory mechanism of NHE1, structural information including the subunit-subunit interaction is extremely limited. A previous study showed that NHE1 and NHE3 form homo-oligomers by interacting via the transmembrane regions in intact cells (*9*), and consistent with this, NHE1 in the placental brush border membranes was detected as a larger form (~205 kDa), cross-linked by disulfide bonds (*10*). Furthermore, we recently presented evidence that NHE1 forms a homodimer but not a homotrimer or a homotetramer (*11*). Despite detailed descriptions of the oligomeric state of the exchanger, its functional significance is not well understood. The previous study (*9*) suggested that the functional unit of NHE1 is a monomer on the basis of the coexpression experiment of transport-deficient mutant E262I. However, it has been reported that the interaction between

[†] This work was supported by a Grant-in-Aid for Priority Areas 13142210 for Scientific Research from the Ministry of Education, Science Culture of Japan, by Grant nano-001 for Research on Advanced Medical Technology from the Ministry of Health, Labor, and Welfare of Japan, and by the Program for Promotion of Fundamental Studies in Health Science of the National Institute of Biomedical Innovation (NIBIO).

* To whom correspondence should be addressed. Tel: 81-6-6833-5012. Fax: 81-6-6835-5314. E-mail: wak@ri.ncvc.go.jp.

[1] Abbreviations: NHE, Na^+/H^+ exchanger; pH_i, intracellular pH; EL, extracellular loop; IL, intracellular loop; TM, transmembrane spanning region; ER, endoplasmic reticulum; MTS-2, 1,2-ethanediyl-bis-methanethiosulfonate; MTS-6, 1,6-hexanediyl-bis-methanethiosulfonate; MTS-17, 3,6,9,12,15,-pentaoxaheptadecane-1,17-diyl-bis-methanethiosulfonate; MTSET, 2-(trimethylammonium) ethyl methanethiosulfonate; PMA, phorbol 12-myristate 13-acetate; EIPA, 5-(*N*-ethyl-*N*-isopropyl)amiloride; NHS-LC-biotin, succinimidyl-6-(biotinamide)-hexanoate; $DiOC_6(3)$, 3,3′-dihexyloxacarbocyanine iodide; BCECF-AM, 2′,7′-bis-(2-carboxyethyl)-5(6)-carboxyfluorescein acetoxymethyl ester; HA, hemaglutinin; PCR, polymerase chain reaction; DMEM, Dulbecco's modified Eagle's medium; HEPES, 2-[4-(2-hydroxyethyl)-1-piperazinyl]ethanesulfonic acid; Tris, Tris(hydroxymethyl)aminomethane; EDTA, ethylenediamine-*N*,*N*,*N*′,*N*′-tetraacetic acid; PBS, phosphate-buffered saline; PAGE, polyacrylamide gel electrophoresis; SH, sulfhydryl; LDS, lithium dodecylsulfate; CCD, charge coupled device; aa, amino acid.

10.1021/bi0608616 CCC: $33.50 © 2006 American Chemical Society
Published on Web 10/17/2006

subunits may be required for NHE1 function using several kinetic approaches (*12*−*14*). In addition, the sigmoidal cytosolic H^+ dependence has recently been reported to be best explained by an allosteric model involving the cooperative interaction between subunits (*14*).

In this study, we have addressed whether dimerization is responsible for the activity of NHE1. We found that expression of a dominant-negative mutant exchanger greatly inhibited the exchange activity in the neutral pH_i range by inducing an acidic shift of the pH_i dependence. Furthermore, the exchange activity was markedly reduced by intermolecular cross-linking between engineered cysteine residues, suggesting that cross-linking restricts the cooperative movement between NHE1 subunits and thereby inhibits ion transport. The present findings provide a strong piece of evidence that dimerization is required for the physiological function of NHE1.

EXPERIMENTAL PROCEDURES

Antibodies and Other Materials. The polyclonal antibody against human NHE1 has been described previously (*15*). Antibodies against HA (3F10) and c-Myc epitopes were purchased from Roche Diagnostics GmbH (Germany) and Santa Cruz Biotechnology, Inc. (CA), respectively. Cysteine-modifier reagent MTSET and cross-linkers MTS-2, MTS-6, and MTS-17 were purchased from Toronto Research Chemicals, Inc. (Canada). $^{22}NaCl$ and [^{14}C]-benzoic acid were purchased from Perkin-Elmer Life Science, Inc. (MA). All other chemicals were of the highest purity available.

Cell Culture and Plasmid DNA Transfection. The exchanger-deficient cell line (PS120) (*16*) and corresponding transfectants were maintained in DMEM containing 25 mM $NaHCO_3$ and supplemented with 7.5% (v/v) fetal calf serum, penicillin (50 units/mL), and streptomycin (50 μg/mL). Cells were maintained at 37 °C in the presence of 5% CO_2. All cDNA constructs were transfected into PS120 or CCL39 cells using the calcium phosphate-DNA coprecipitation technique or with Lipofectamine 2000 (Invitrogen Corp., CA), and stable clones for NHE1 and mutant constructs were selected by repetitive H^+-killing selection procedures, as described previously (*17*). In some cases, G418-resistant cell clones were isolated.

Construction of the NHE1 Mutant Plasmid. A plasmid carrying a cDNA encoding human NHE1 and containing unique restriction sites cloned into the mammalian expression vector pECE has been described previously (*17*). A cDNA construct for NHE1 in which all endogenous cysteine residues were replaced by alanine, designated as Cys-less NHE1, has also been described previously (*18*). Construction of plasmids for NHE1 containing point mutations was carried out by a PCR-based strategy using two template plasmids encoding wild-type or Cys-less NHE1, as described previously (*18*). Similarly, plasmids containing nucleotide sequences corresponding to the HA epitope YPYDVPDYAS or the c-Myc epitope EQKLISEEDL were constructed by inserting PCR fragments produced using antisense primers containing either epitope sequence and a stop codon just after the *C*-terminus of NHE1 into the appropriate restriction sites of the plasmid containing NHE1 cDNA. Constructs were confirmed by sequencing plasmids with an ABI-PRISM DNA sequencer model 3100 (Applied Biosystems, CA). In this study, we use the prefix "cl-" for point mutants produced from Cys-less NHE1 as background.

Cross-Linking between Cysteine Residues of NHE1. The cross-linking reaction was performed using PS120 cells stably expressing the NHE1 mutants, essentially as described previously (*11*). Cells expressing each mutant containing a single cysteine residue at an extracellular site of Cys-less NHE1 were grown to confluence, usually on a 12-well plate, and then were washed twice with balanced salt solution (BSS) containing 136 mM NaCl, 4 mM KCl, 1 mM $MgCl_2$, 1.8 mM $CaCl_2$, 5 mM glucose, and 10 mM HEPES at pH 7.4 adjusted with NaOH. Cells were then treated with various thiol-specific cross-linkers, MTS-2, MTS-6, and MTS-17 (usually 0.1−1.0 mM), in the above solution for 15 min at room temperature. The cross-linking reaction was stopped by the addition of 300 μL of 2× LDS sample buffer (Invitrogen) containing 10 mM *N*-ethylmaleimide per well, and then the PAGE mobility of NHE1 variants in the samples was analyzed by immunoblotting.

Immunoprecipitation and Immunoblotting. For co-immunoprecipitation of the Myc-tagged wild-type NHE1 and the HA-tagged E262I mutant, cells coexpressing these proteins were washed with ice-cold PBS and solubilized with lysis buffer (1% Triton X-100, 5 mM EDTA, 1 mM phenylmethylsulfonyl fluoride, and 1 mM benzamidine in PBS) for 20 min on ice. Quantitative analysis revealed that most of NHE1 (88 ± 4%) was recovered in the Triton-soluble fraction. After centrifugation for 5 min at 15,000 rpm, the supernatant (Triton-soluble fraction) was incubated for 2 h at 4 °C with rabbit anti-Myc antibody plus 30 μL of Protein A-Sepharose beads (Amersham Biosciences, Inc., NJ). The beads were washed five times with ice-cold lysis buffer, and proteins were eluted with LDS sample buffer containing 50 mM DTT. After PAGE on 3−8% gradient gels (NuPAGE Gel, Invitrogen), proteins were transferred electrophoretically onto polyvinylidene difluoride membranes and subjected to immunoblotting with anti-HA. Proteins were visualized by enhanced chemiluminescence detection (Amersham).

Immunocytochemistry. Cells were fixed with cold methanol and then blocked with PBS containing 5% BSA fraction IV. Cells were then treated with anti-NHE1 or anti-HA antibody followed by fluorescent staining with a rhodamine-labeled secondary antibody. Fluorescent images were taken using a confocal laser scanning attachment (MRC1024, BioRad) mounted on an upright microscope (BX50WI, Olympus Corp., Japan) equipped with an 60× water immersion objective (LUMPlanFI, Olympus). Both the anti-NHE1 antibody and the secondary antibody were used after absorbing against PS120 cells. All procedures were performed at room temperature.

Surface Labeling. Cells were incubated with 1 mM NHS-LC-Biotin (Pierce Biotechnology, IL) in PBS containing 0.1 mM $CaCl_2$ and 1 mM $MgCl_2$ for 30 min at room temperature and then solubilized with lysis buffer. The lysate was centrifuged to remove the insoluble fraction. The supernatant was incubated with streptavidin-agarose beads (Pierce) for 1 h at 4 °C, and the beads were then washed five times with lysis buffer. The proteins were eluted with 2× LDS sample buffer by heating and then subjected to immunoblot analysis.

Measurement of ^{22}Na Uptake. $^{22}Na^+$ uptake activity was measured by the K^+/nigericin pH_i clamp method (*19*). Briefly, serum-depleted cells in 24-well plates were preincubated

for 30 min at 37 °C in a Na^+-free choline chloride/KCl medium containing 20 mM HEPES/Tris (pH 7.4), 1.2−140 mM KCl, 2 mM $CaCl_2$, 1 mM $MgCl_2$, 5 mM glucose, and 5 μM nigericin (Invitrogen). $^{22}Na^+$ uptake was started by adding the same choline chloride/KCl solution containing $^{22}NaCl$ (37 kBq/mL: final concentration, 1 mM), 1 mM ouabain, and 0.1 mM bumetanide. In some wells, the uptake solution contained 0.1 mM EIPA. One to 5 min later, cells were rapidly washed four times with ice-cold PBS to terminate $^{22}Na^+$ uptake. pH_i was calculated from $[K^+]_i/[K^+]_o = [H^+]_i/[H^+]_o$ by assuming an intracellular $[K^+]$ of 120 mM. In some experiments, cells were treated with MTS cross-linkers for 15 min at room temperature prior to incubation with pH_i-clamp buffer. The data were normalized on the basis of protein concentration, which was measured using a bicinchoninic assay system (Pierce), using bovine serum albumin as a standard.

Intracellular pH Measurement. Cells were seeded onto 22-mm glass coverslips coated with collagen Type-I (BD Biosciences, NJ). Two days after plating, cells were loaded with 1 μM BCECF/AM (Invitrogen) in a "Na^+ solution" containing 10 mM HEPES/Tris (pH 7.4), 136 mM NaCl, 4 mM KCl, 1.8 mM $CaCl_2$, 1 mM $MgCl_2$, and 5 mM glucose for 10 min at room temperature. The coverslip was mounted on a flow chamber and continuously perfused with solution at 0.6 mL/min by means of a Perista pump (ATTO Corp., Japan). Changes in pH_i were estimated by ratiometric imaging of changes in BCECF fluorescence. Fluorescence was monitored at 510−530 nm by alternatively exciting at 440 and 490 nm through a 505-nm dichroic reflector. Fluorescence images were collected every 5 or 10 s using a cooled CCD camera (ORCA-ER, Hamamatsu photonics K.K., Japan) mounted on an inverted microscope (IX 71, Olympus) with an 20× objective (UApo/340, Olympus) and then were processed with AQUACOSMOS software (Hamamatsu photonics). For NH_4 prepulse, cells were perfused for 5 min with the above Na^+ solution containing 30 mM NH_4Cl, followed by perfusion with a Na^+-free solution (NaCl was replaced by choline Cl). The NHE1-dependent pH_i recovery was induced by reperfusion with the Na^+ solution. The pH_i value was calibrated using a "high K^+ solution" containing 5 μM nigericin adjusted to various pH values. The change in pH_i was also measured by the [^{14}C]benzoic acid-equilibration method (*17*). In this experiment, serum-depleted cells were preincubated for 30 min in bicarbonate-free HEPES-buffered DMEM (pH 7.0) and then incubated in the same medium containing [^{14}C]benzoic acid (1 μCi/mL) for 10 min at 37 °C. After washing four times with ice-cold PBS, the cellular uptake of ^{14}C-radioactivity was measured. The change in pH_i was calculated as described previously (*17*).

RESULTS

Heterodimer Formation between the Wild-Type and Inactive Mutant Exchangers. In this study, we constructed two NHE1 mutants, G309V and E262I (see Figure 1A for their positions in the secondary structure of NHE1). These mutant exchangers showed no EIPA-sensitive $^{22}Na^+$ uptake activity when they were expressed in exchanger-deficient PS120 cells (Figure 1B). Although the fully glycosylated mature form of the wild-type and E262I exchangers were recognized in the immunoblot with anti-NHE1 antibody (Figure 1C), only the immature form of G309V was observed in the immunoblot, suggesting that G309V may be retained in the intracellular membranes. In order to check the surface expression of these mutant exchangers, we carried out the immunofluorescence analysis with anti-NHE1 antibody. Similar to the wild-type NHE1, E262I tagged with HA were expressed at least partly in the plasma membrane, as shown by immunofluorescence observation with anti-HA antibody (Figure 2A; see inset for the fluorescence intensity profile analysis). In contrast, most of G309V proteins were retained in the intracellular membranes (Figure 2A and B for summarized data). Furthermore, G309V proteins were mostly co-stained with the ER marker $DiOC_6(3)$, whereas neither the wild-type nor the E262I exchangers were co-stained (Figure 2C). Thus, the lack of exchange activity of G309V could result from no surface expression of this mutant.

In order to examine whether the G309V mutant interacts with the wild-type NHE1 and thus inhibit its plasma membrane trafficking, we isolated a stable cell line expressing

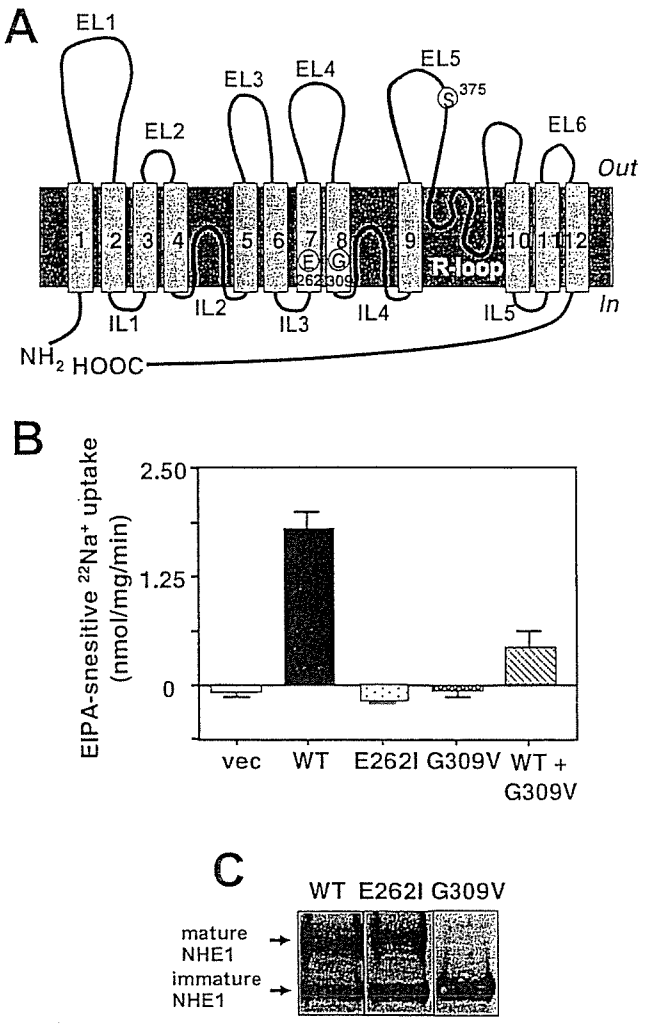

FIGURE 1: Characterization of two inactive mutant exchangers. (A) Secondary structure model of NHE1. The membrane topology has previously been determined by cysteine-accessibility analysis (*18*). Relative positions of mutated residues (Glu^{262}, Gly^{309}, and Ser^{375}) are indicated in the Figure. R-loop, reentrant loop. (B) EIPA-sensitive $^{22}Na^+$-uptake activity in PS120 cells transiently transfected with an empty pECE vector (vec), wild-type NHE1 (WT), E262I, G309V, or wild-type NHE1 plus G309V (0.3 μg for each). Values are the means ± S.D. of triplicate determinations. (C) Immunoblots of proteins obtained from cells stably expressing the wild-type, E262I, or G309V. Cell lysate proteins (50 μg/lane) were applied to 3−8% SDS-PAGE and visualized with anti-NHE1 antibody.

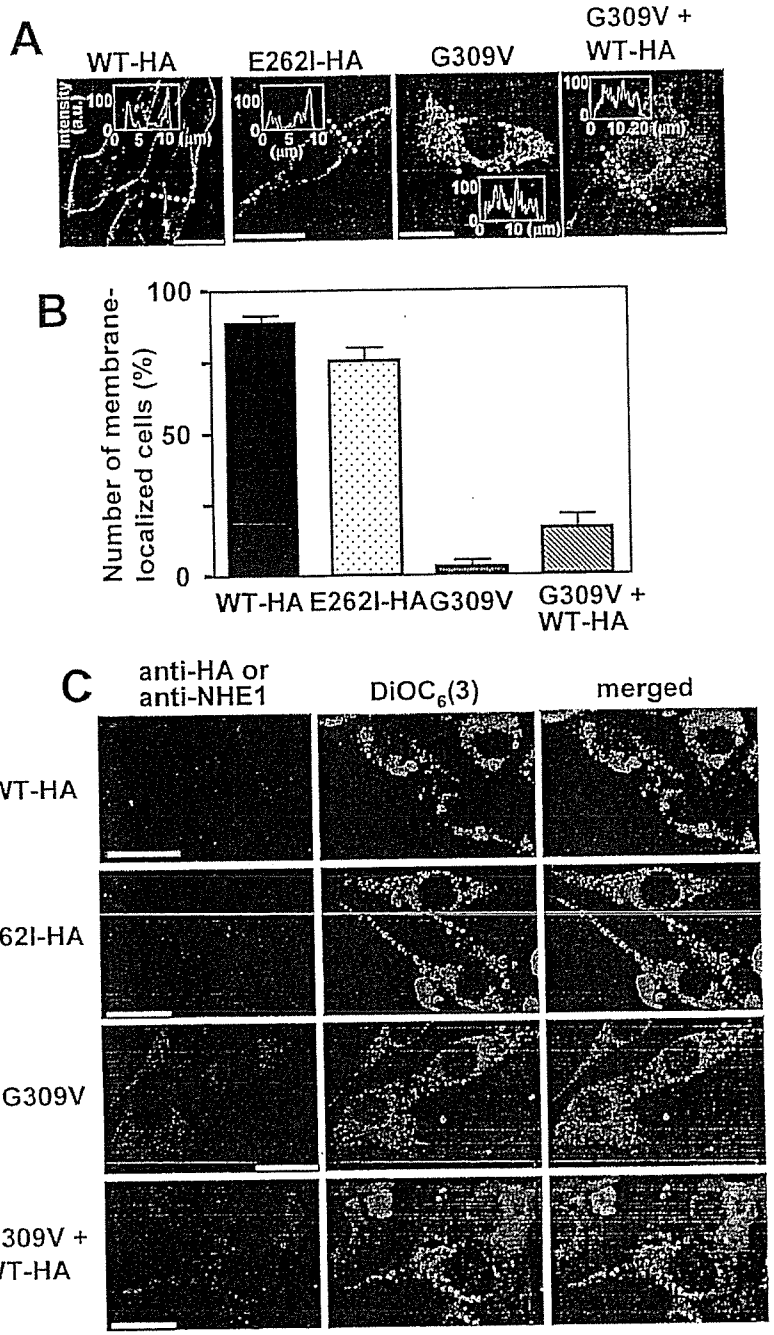

FIGURE 2: Immunofluorescence analysis of two mutant exchangers. (A) Confocal immunofluorescence images of the cells stably expressing the NHE1 variants with or without HA-tag. In one experiment (right panel), cells stably expressing G309V were further transfected with NHE1-HA. Cells were immunostained with anti-HA except for G309V, which were immunostained with anti-NHE1 (third panel). The inset shows the intensity profile of fluorescence along the dotted line. In many cells expressing the wild-type or E262I mutant exchangers, strong fluorescence signals were detected at the cell edge. (B) Summary data for membrane localization of fluorescence signal. The number of cells with a strong fluorescence signal at the cell edge (at least three times more than the average of fluorescence in the internal cell region) was counted. Data are expressed as the mean ± S.D. from six images (total cell number analyzed, 39−101). (C) Double staining of cells for NHE1 and ER maker $DiOC_6$ (3). Cells were fixed, permeabilized, and immunostained with anti-HA or anti-NHE1 antibody for G309V (left panels) and then briefly (1 min) incubated with the ER marker $DiOC_6(3)$ (0.1 μM) (middle panels). These fluorescent images were merged (right panels). Scale bars, 20 μm.

G309V and then transfected these cells with HA-tagged wild-type NHE1. In contrast to the predominant localization of the wild-type NHE1 in the plasma membrane upon transfection with a NHE1-carrying vector alone (Figure 2C, left top panel), coexpression of G309V markedly inhibited the surface expression of NHE1 (Figure 2C, left bottom panel and see also Figure 2A and B). Consequently, most of this wild-type NHE1 proteins were retained in the ER, which were co-stained with $DiOC_6(3)$ upon expression of G309V (Figure 2C, right bottom panel). Coexpression also resulted in a strong dominant-negative effect of G309V on exchange activity, as assessed by $^{22}Na^+$ uptake (Figure 1B). Therefore, it is likely that G309V is able to form a heterodimer with the wild-type NHE1 and that dimerization of NHE1 may first occur in the ER membranes, although we do not exclude the possibility that NHE1 subunits interact indirectly.

We next examined whether the wild-type and E262I exchangers exist as a heterodimer in the plasma membrane. We stably coexpressed E262I tagged with an HA epitope (E262I-HA) and the wild-type NHE1 tagged with a Myc

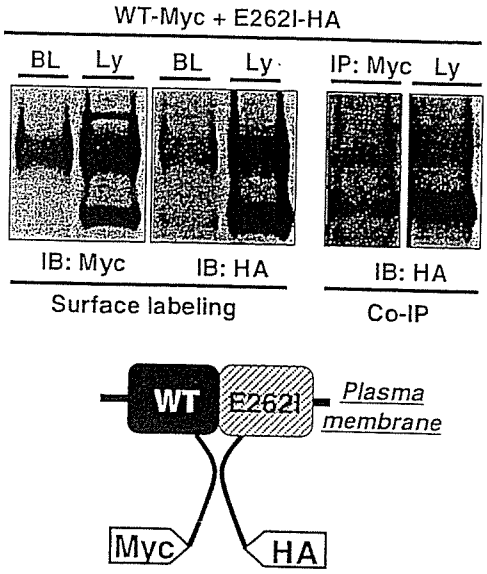

FIGURE 3: Heterodimer formation between the wild-type NHE1 and E262I in the plasma membrane. Cells were stably cotransfected with Myc-tagged NHE1 and HA-tagged E262I and treated with 1 mM NHS-LC-biotin. The biotin-labeled proteins (BL) were collected with streptavidin-agarose beads and analyzed by immunoblotting. Double-transfected cells were also solubilized and subjected to immunoprecipitation with anti-Myc antibody, followed by immunoblotting with anti-HA antibody. The cell lysate was also analyzed by immunoblotting with the indicated antibodies (Ly).

epitope (WT-Myc) in PS120 cells. Cells were surface labeled with NHS-LC-biotin, and biotinylated proteins were recovered with streptavidin-agarose and then analyzed by immunoblotting with anti-HA or anti-Myc antibodies. The results indicate that both proteins were surface-biotinylated (Figure 3), that is, expressed in the plasma membrane. The immature E262I protein band slightly detected in the biotin-treated fraction may be due to the partial membrane permeability of NHS-LC-biotin. To semiquantitatively evaluate the surface expression of NHE1, we estimated the amount of NHE1 proteins adsorbed by streptavidin-agarose beads by subtracting the amount of unbound NHE1 (including immature NHE1) from that of total NHE1 after incubation with beads (data not shown). From such an analysis, we concluded that 45.4 ± 8.7 and 33.3 ± 13.2% (means ± S.D., $n = 3$) of total NHE1 proteins were adsorbed by the beads, that is, expressed in the cell surface for the wild-type and E262I exchangers, respectively. Furthermore, co-immunoprecipitation analysis revealed that E262I-HA was detected in the immunoprecipitates with anti-Myc antibody (Figure 3), suggesting that the Myc-tagged wild-type NHE1 and HA-tagged E262I interact with each other. Hence, surface-labeling and co-immunoprecipitation experiments indicate that wild-type NHE1 forms a heterodimer with E262I in the plasma membrane.

Coexpression of Transport-Deficient NHE1 Mutant Exerts a Dominant-Negative Effect in the Neutral pH_i Range. We next examined the effect of the expression of E262I on the exchange activity of NHE1. We expected that if two active subunits are required for the exchange reaction, heterodimer formation between the wild-type and E262I exchangers would result in the inhibition of activity via the dominant-negative effect of E262I. PS120 cells were transiently transfected with plasmids carrying wild-type NHE1 together with the E262I mutant or an empty vector at a molar ratio of 1:1

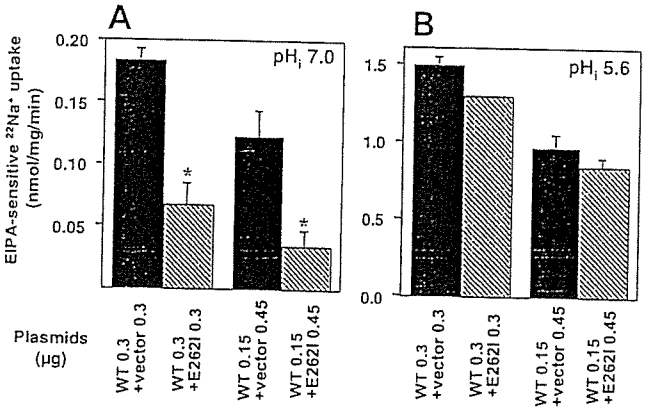

FIGURE 4: Dominant negative effect of E262I on the exchange activity of NHE1. Plasmids carrying the wild-type NHE1 (WT) or E262I were transiently cotransfected into PS120 cells plated on a 24-well plate using Lipofectamine2000. The total quantity of plasmids transfected per well was adjusted to 0.6 μg. In the absence of the E262I plasmid, the total quantity was adjusted with an empty vector. The ratio of the transfected plasmid (WT/E262I or WT/empty vector) was 1:1 and 1:3. Two days after transfection, EIPA-sensitive $^{22}Na^+$ activity was measured at pH_i 7.0 (A) or 5.6 (B) clamped by K^+-nigericin, as described under Experimental Procedures. Values are the means ± S.D. of triplicate determinations. The statistical significance of the data was analyzed by unpaired *t*-test. $^*P < 0.05$.

or 1:3, and exchange activities were assessed by measuring EIPA-sensitive $^{22}Na^+$ uptake at both neutral (7.0) and acidic pH_i (5.6). As shown in Figure 4A, coexpression of E262I resulted in a marked reduction of the activity of the wild-type NHE1 at pH_i 7.0 (more than 50% reduction), that is, E262I exerted the dominant-negative effect. In contrast, expression of E262I had a negligible effect on the exchange activity at acidic pH_i (Figure 4B). These results suggest that heterodimerization with E262I inhibits the transport activity of NHE1 in a pH_i-dependent manner.

We further investigated the dominant-negative effect of E262I under more physiological conditions. To do this, we used CCL39 fibroblastic cells because these cells homogenously express a relatively low amount of endogenous NHE1. The plasmid carrying E262I was cotransfected with DsRed vector carrying a red fluorescent protein as an expression marker. After DsRed fluorescent images were taken, cells were loaded with a fluorescent pH_i indicator, BCECF-AM. Figure 5A shows typical images of DsRed (b) and BCECF fluorescence (c), which were taken in an identical microscopic field. Using this system, the NHE activity was assessed by measuring pH_i recovery after NH_4^+ prepulse. The DsRed-negative cells exhibited a relatively rapid pH_i recovery due to endogenous NHE1 (see cell number 4 in Figure 5A and B). In contrast, the pH_i-recovery rate was dramatically reduced in E262I-expressing DsRed-positive cells (cells numbered 1, 2, and 3). The data from DsRed-positive cells are collected and summarized in Figure 5C and D. While transfection of exogenous wild-type NHE1 accelerated the rate of pH_i recovery, expression of E262I greatly reduced it (Figure 5C and D). Furthermore, expression of E262I shifted the pH_i dependence of the recovery rate to the acidic side (Figure 5E). Figure 5F shows the change in pH_i in response to thrombin. In vector-transfected control CCL39 cells, thrombin induces a rapid cytoplasmic alkalinization via the activation of NHE1, preceded by the transient acidification (asterisk) resulting from Ca^{2+}-

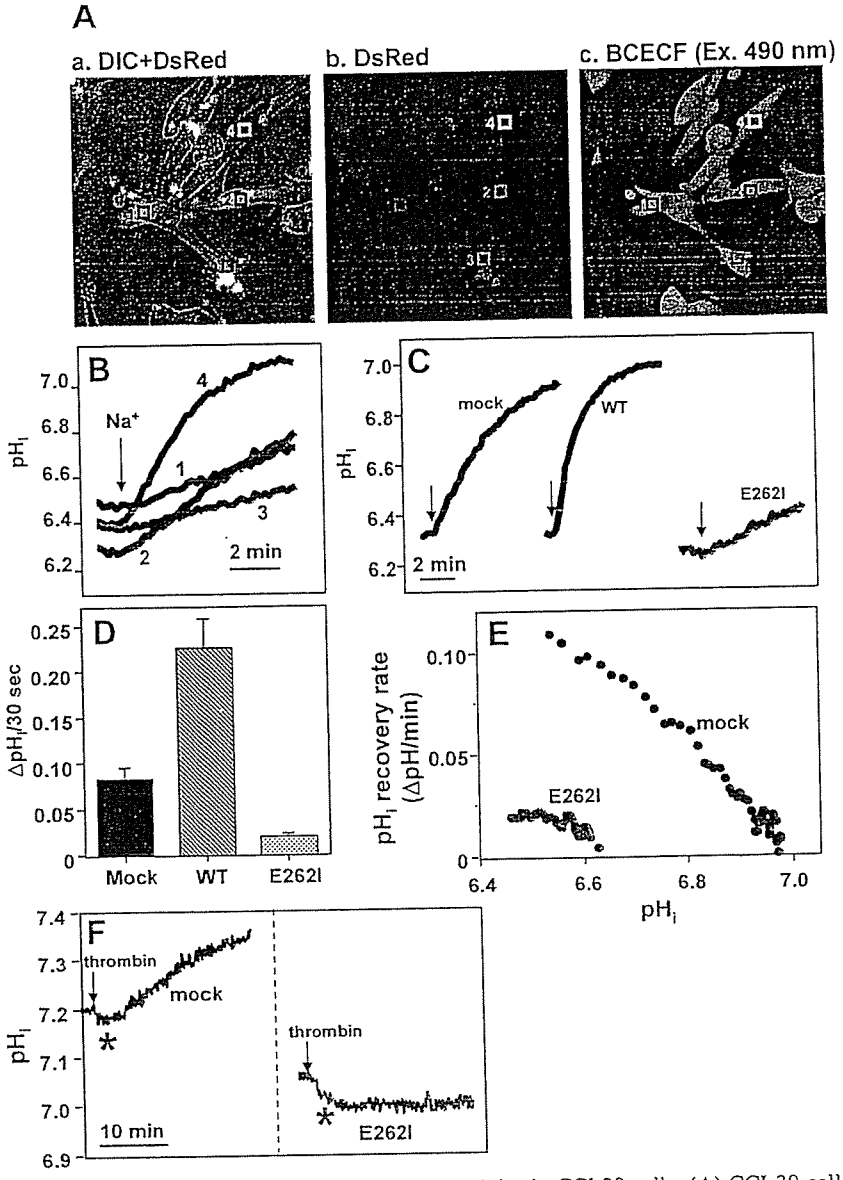

FIGURE 5: Dominant−negative effect of E262I on endogenous NHE1 activity in CCL39 cells. (A) CCL39 cells were grown on collagen-coated glass coverslips and transiently cotransfected with E262I and DsRed (as an expression marker) at a molar ratio of 3:1. Forty-eight hours after transfection, they were serum-depleted for more than 5 h, and a coverslip with a perfusion chamber was mounted on the stage of an inverted microscope fitted with a CCD camera. Differential interference contrast (DIC) and DsRed fluorescence images (a and b) were taken, and then the cells were loaded with 3 μM BCECF-AM for 10 min at room temperature (c, BCECF fluorescence image). (B) pH_i-recovery curves obtained from individually numbered cells. The numbers in B correspond to those in A. Na^+ was added at the time shown by the arrow. (C) and (D) Cells were transiently cotransfected with DsRed together with empty vector (mock), wild-type NHE1, or E262I plasmid, and pH_i-recovery curves were obtained from a DsRed-positive cell. Data were collected from more than 60 DsRed-positive cells in two independent experiments, and a summary of these data is shown. In C, these averaged pH_i-recovery curves are shown, whereas in D, the pH_i increment during 30 s starting from pH_i 6.3 (means ± S.E.) is shown. (E) pH_i dependence of pH_i-recovery rates. The averaged rate of pH_i recovery (C) was calculated from the pH_i increment at every 10 s and plotted against pH_i. (F) Change in pH_i in response to thrombin. CCL39 cells were transiently cotransfected with an empty vector or E262I together with DsRed. At the time indicated by arrows, perfusion was changed to the solution containing 1 uint/mL thrombin. Traces from more than 60 cells were averaged. Asterisks (*) represent the transient acidification resulting from intracellular Ca^{2+} mobilization. These acidifications suggest that cells are capable of undergoing normal cell signaling in response to thrombin.

mobilization (*1*). The expression of E262I completely inhibited this thrombin-induced cytoplasmic alkalinization. Thus, expression of E262I strongly inhibits endogenous NHE1 activity in CCL39 cells in the neutral pH_i range, and thereby abolishes the pH_i regulation in response to growth factors. It should be noted that unlike the $^{22}Na^+$ uptake measurement, we could not assess the exchange activity at very acidic pH_i by measuring pH_i recovery because it was difficult to acidify cells by less than 6.0 by NH_4^+ prepulse.

Na^+/H^+ Exchange Activity Is Inhibited by Symmetrical Intermolecular Cross-Linking at External Cysteine Residues. We expected that if dimerization is essential for the function of NHE1, cross-linking between the two NHE1 subunits would inhibit the Na^+/H^+ exchange reaction by restricting the conformational change of the proteins during transport. We constructed NHE mutants containing a single cysteine using Cys-less NHE1 as a background. Of the 34 single cysteine mutants tested, we found that symmetrical cross-

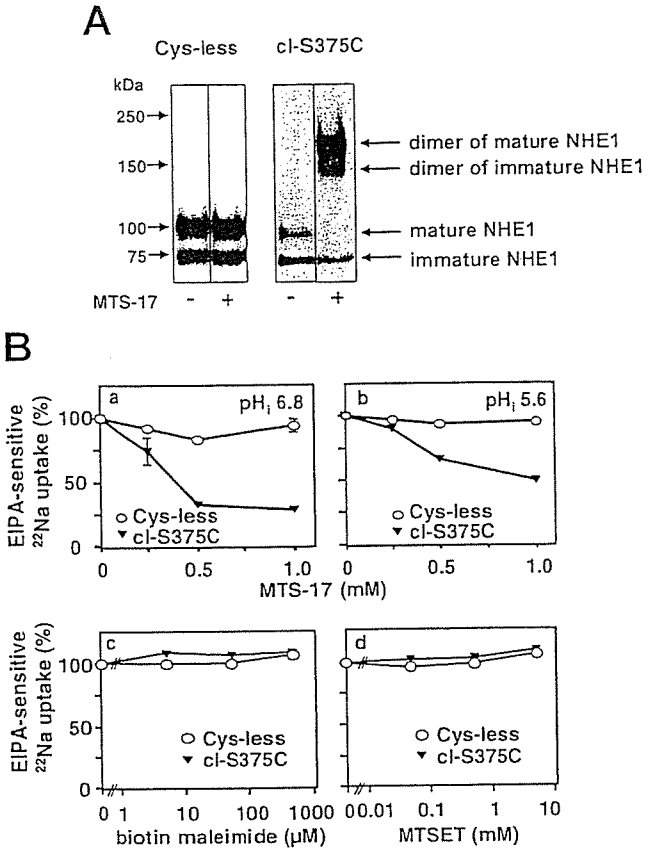

FIGURE 6: Inhibition of NHE1 activity by treatment with cross-linkers. (A) Immunoblot analysis representing the intermolecular cross-linking of cl-S375C proteins. Cells stably expressing Cys-less NHE1 (left panel) or cl-S375C (right panel) were treated with 1 mM MTS-17 for 15 min at 4 °C in BSS and subjected to immunoblot analysis with anti-NHE1 antibody. (B) Cells expressing Cys-less NHE1 or cl-S375C were grown to confluence in 24-well dishes and treated with the indicated concentrations of MTS-17, biotin maleimide, or MTSET for 15 min at room temperature, and the $^{22}Na^+$-uptake activity was measured. In the absence of modifying reagents, EIPA-sensitive $^{22}Na^+$-uptake activity was 10−15 and 40−50 nmol/mg/min at pH$_i$ 6.8 and 5.6 for Cys-less and cl-S375C mutants, respectively. Data were normalized by the values without modifying reagents and represented as means ± S.D. of triplicate determinations. Error bars are sometimes smaller than symbol sizes.

linking occurred with homobifunctional MTS cross-linkers, MTS-2, MTS-6, or MTS-17, at six extracellular sites of NHE1, Pro^{153} in extracellular loop (EL) 2, Asn^{282} and Tyr^{283} in EL4, and Ser^{375}, Thr^{377} and Tyr^{381} in EL5. In this study, we focused on a mutant cl-S375C because a significant reduction of activity was observed upon cross-linking in this mutant. Treatment of the cells with MTS-17 resulted in a mobility shift of cl-S375C from the monomer to the dimer position (right panel of Figure 6A). Immature NHE1 is also cross-linked, as shown by the mobility shift of the lower bands. A similar mobility shift was also observed on treatment with MTS-2 or MTS-6 having shorter spacer arms (data not shown). In contrast to cl-S375C, such a mobility shift was not observed in Cys-less NHE1 (Figure 6A). We investigated whether cross-linking actually affects NHE activity by assessing the effects of cross-linking reagents on EIPA-sensitive $^{22}Na^+$ uptake. Although treatment with MTS-17 had no effect on the activity of Cys-less NHE1, the same treatment markedly suppressed the activity of cl-S375C in a dose-dependent manner both at neutral (6.8) and low pH$_i$ (5.6) (Figure 6B, a and b). Similarly, inhibition of NHE1 activity was also observed as a decrease in the rate of pH$_i$ recovery after acid loading (data not shown). In contrast to MTS-17, the activity was not affected by the monofunctional SH-modifier reagents biotin maleimide or MTSET (Figure 6B, c and d), which have been reported to react with a cysteine residue at position Ser^{375} (*18*), suggesting that inhibition of cl-S375C activity by MTS-17 is not simply due to SH-modification but to intermolecular cross-linking. We did not examine the effects of MTS-2 or MTS-6 on exchange activity because these reagents had a severe toxic effect on cells.

We next investigated several functional properties of cross-linked cl-S375C. As shown in Figure 6B, inhibition of the cl-S375C activity by cross-linking was stronger at high pH$_i$ (75% inhibition at pH$_i$ 6.8) compared to that at low pH$_i$ (50% inhibition at pH$_i$ 5.6). Consistent with this finding, cross-linking with MTS-17 greatly shifted the pH$_i$ dependence of $^{22}Na^+$ uptake to the acidic side and virtually abolished the activity in the neutral pH$_i$ range (Figure 7A), although amino acid substitution of Ser^{375} itself also slightly shifted the pH$_i$ dependence to the acidic side (data not shown). The pH$_i$ dependence of $^{22}Na^+$-uptake activity in Cys-less NHE1 was not affected by treatment with MTS-17 (data not shown). In addition, in cells expressing cl-S375C, cytoplasmic alkalinization in response to thrombin, PMA, or hyperosmotic stress was completely abolished upon treatment with MTS-17 (Figure 7B), whereas significant alkalinization was observed in Cys-less NHE1 (Figure 7B). Lack of NHE1 activation in response to extracellular stimuli is probably due to an acidic shift of the pH$_i$ dependence caused by treatment with MTS-17. In contrast to pH$_i$ regulation, cross-linking with MTS-17 exerted only a small effect on the concentration dependence of extracellular Na^+ (Figure 7C). The K_m values for Na^+ were 8.33 ± 0.64 and 8.95 ± 0.50 mM in Cys-less NHE1 (the trace is not shown) and 12.7 ± 0.7 and 7.99 ± 1.15 mM in cl-S375C in the control and MTS-treated cells, respectively. Treatment with MTS-17 slightly reduced the sensitivity to inhibitor EIPA in cl-S375C (Figure 7D), whereas the same treatment had no effect on EIPA inhibition in Cys-less NHE1 (data not shown). The EIPA concentrations giving half-maximal inhibition (IC_{50}) were 78.23 ± 1.56 and 88.1 ± 11.3 nM in Cys-less NHE1 and 126.0 ± 10.3 and 198 ± 10.6 nM in cl-S375C in control and MTS-treated cells, respectively. These results suggest that cross-linking at extracellular sites has a large influence on exchanger function across the membrane, while exerting a moderate effect on the affinities for extracellular Na^+ and EIPA.

DISCUSSION

In this work, we analyzed the functional significance of the dimerization of NHE1 by means of the expression of a dominant-negative mutant exchanger and intermolecular cross-linking. Initially, we showed that the wild-type NHE1 is capable of interacting with surface expression-deficient G309V and with transport-deficient E262I. These observations, together with the data from cross-linking experiment, reinforce the previous findings that NHE1 exists as a dimer in plasma membranes. Experiments with the dominant-negative mutant NHE1 provided evidence that two active subunits are required for the function of NHE1. The expres-

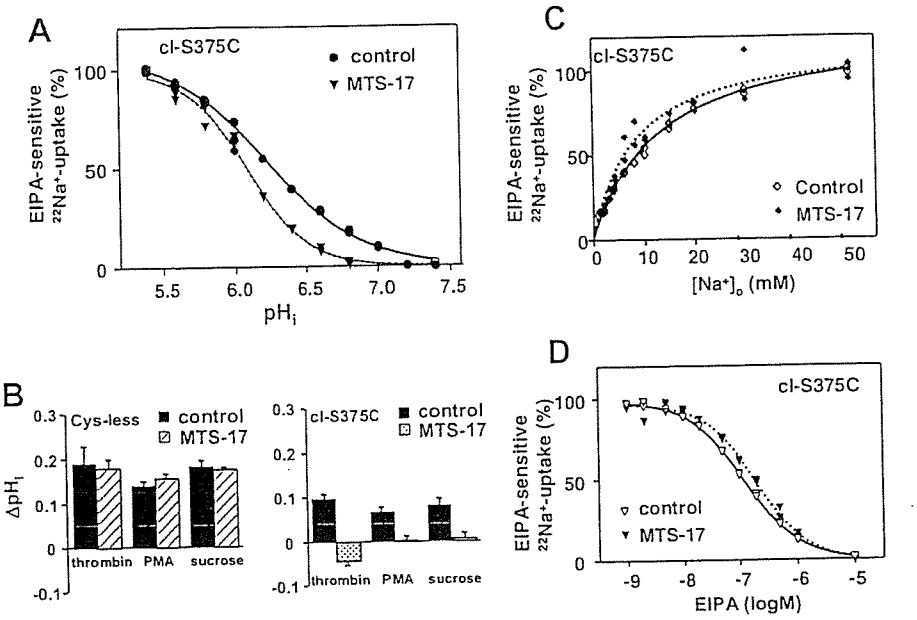

FIGURE 7: Functional properties of cl-S375C after cross-linker treatment. (A) pH_i dependence of EIPA-sensitive $^{22}Na^+$-uptake activity measured in cells expressing cl-S375C treated with or without MTS-17. The $^{22}Na^+$ uptake at pH_i 5.4 was reduced after cross-linker treatment (Figure 6B). Data were normalized to those at pH_i 5.4. (B) Change in pH_i in response to various external stimuli. Cells expressing Cys-less NHE1 or cl-S375C were incubated with or without 250 μM MTS-17 for 15 min at room temperature, and then the external stimuli-induced change in pH_i was measured using the [^{14}C]benzoic acid-equilibration method as described in Experimental Procedures. Cells were stimulated with 1 unit/mL thrombin, 1 μM PMA, or 200 mM sucrose (hyperosmotic stress). (C) and (D) Effect of MTS-17 on the concentration dependences of EIPA-sensitive $^{22}Na^+$ uptake on external Na^+ ($[Na^+]_o$) and EIPA in cells expressing cl-S375C. Cells were treated with 500 μM MTS-17 for 15 min at room temperature and pH_i-clamped at 5.6, and then the $^{22}Na^+$ uptake was measured in the presence of various concentrations of Na^+ (C) or EIPA (D). Data were normalized by the values at 50 mM Na^+ for C or at 1 nM EIPA for D.

sion of transport-deficient E262I in CCL39 cells dramatically reduced the exchange activity of endogenous NHE1 through an acidic shift in the pH_i dependence of exchange activity (Figure 5). In addition, coexpression of E262I, together with wild-type NHE1, markedly reduced exchange activity at neutral pH_i, whereas it exerted only a marginal effect on the activity at acidic pH_i (Figure 4). These data suggest that heterodimer formation between the wild-type protein and the E262I mutant exchanger results in a marked inhibition of exchange activity by inducing an acidic shift of the pH_i dependence, suggesting that dimerization would be essential for physiological exchange activity.

Secondary active transporters such as NHE1 are generally thought to have two major alternating conformations during the transport cycle, outward- and inward-facing orientations. This is also compatible with the recently solved crystal structures of two major facilitator superfamily transporters, the glycerol-3-phosphate transporter (*20*) and the lactose permease of *E. coli* (*21*). In the E262I subunit of the NHE1 heterodimer, such a conformational change may not be able to take place because this subunit is transport-deficient. Therefore, it is possible that the fixed structure of E262I restricts the free motion of a neighboring active subunit. Intermolecular cross-linking would provide another approach to restrict such motion between subunits. The treatment of cells expressing cl-S375C with MTS-17 markedly reduced exchange activity. Importantly, this inhibition mainly occurs by shifting the pH_i dependence of exchange to the acidic side and partly by decreasing the maximal activity at acidic pH_i (V_{max}) and consequently abolished extracellular stimuli-induced cytoplasmic alkalinization. The same treatment, however, did not exert a large influence on the apparent affinities for extracellular Na^+ or the inhibitor EIPA. Intermolecular cross-linking at position Ser^{375}, which is located in EL5, occurred upon treatment with all tested MTS reagents. These reagents have different spacer arms (MTS-2, 5.2 Å; MTS-6, 10.4 Å; and MTS-17, 24.7 Å), suggesting that Ser^{375} in EL5 is mobile over a relatively long distance at least between 5 and 25 Å. In membrane transporters, the movement of extracellular loops often plays an important role in the transport cycle. For example, in the glycine transporter GLYT2, the first extracellular loop is reported to alter its accessibility to SH-modification reagents during the transport cycle (*22*). Our data suggest that cross-linking at position Ser^{375} would restrict the motion of EL5 to less than 25 Å between NHE1 subunits and in turn lead to a marked reduction in exchange activity. These results can be explained if it is assumed that dimerization is essential for NHE1 function and that the two NHE1 subunits undergo conformational changes in a concerted manner. Cross-linking would restrict the coupled motion between the subunits, thereby leading to the inhibition of exchange activity possibly by an apparent reduction in pH_i sensitivity. Thus, the data obtained from two different approaches, the dominant-negative experiment and cross-linking, overall suggest that the exchange activity depends on a coupled conformational change of two subunits at physiological pH_i and raise the interesting possibility that the pH-sensing machinery of NHE1 may be fully functional only when two subunits are active. This idea is consistent with previous reports (*12*–*14*) suggesting that subunit-subunit interaction may be important for the function of the exchanger. For example, the Na^+/H^+ exchange in kidney brush border membrane vesicles was reported to exhibit the sigmoidal Na^+ dependence under certain conditions (*12*, *13*). Also, the pH_i dependence of exchange activity was recently reported to be best explained by allosteric kinetics on the basis of the assumption of a dimeric transporter (*14*).

It is of interest to note that inhibition of activity by expression of E262I was not detected at low pH_i (Figure 4), suggesting that the wild-type NHE1 subunit of the heterodimer is functional when intracellular H^+ concentration is sufficiently high. This is consistent with a previous report demonstrating that the dominant-negative effect of E262I on Na^+/H^+ exchange activity was not detected in measurements taken at acidic pH_i (*9*). This observation may be explained if we assume that E262I affects H^+-regulatory sites but not ion-transport sites of the neighboring active subunit. At present, there is substantial evidence that the ion transport machinery is located within the membrane-spanning region. For example, previous studies have shown that mutations of residues within TM4 and TM9 of NHE1 reduce the affinity for Na^+ or the cation transport activity (*23*−*27*). Furthermore, crystal structure determination and mutational studies on the bacterial Na^+/H^+ antiporter NhaA suggest that the ion binding site consists of several polar residues within the transmembrane helices (*28*, *29*). A high-resolution crystal structure of a bacterial Na^+/Cl^--dependent neurotransmitter transporter homologue provided more direct proof that residues within the transmembrane helices coordinate two Na^+ ions (*30*). Thus, it is reasonable to suppose that each subunit of NHE1 has an ion transport pathway and the active subunit of the heterodimer is capable of catalyzing the transport reaction under particular conditions. However, previous biochemical data (*6*, *8*) suggest that the H^+-regulatory sites and ion-transport sites of exchangers are a part of different structural elements and that the acidic shift in the pH_i dependence of exchange mainly results from decrease in the H^+ affinity at regulatory sites. Recent crystal structure determination of NhaA (*28*) and the subsequent electrostatic analysis (*31*) predicted that charged residues with unusual pK_a values, as the pH-sensor, may undergo protonation/deprotonation reactions and subsequently induce the overall conformational changes resulting in the formation of the active form. In the case of NHE1, we have previously identified crucial elements regulating pH sensing: (i) Arg^{440} in IL5 (*32*), (ii) a juxtamembrane cytoplasmic domain (aa 503−595) (*19*), and (iii) a calcineurin B homologous protein (CHP) interacting with a part of this juxtamembrane domain (*33*, *34*). Arg^{327} in IL4 has also recently been reported to be an important residue for determining H^+ affinity (*14*). Interaction with E262I may possibly modify these regions of the neighboring active subunit. Intermolecular cross-linking at position Ser^{375} may also exert similar effects on H^+-regulatory sites. This led us to predict that these important regions of NHE1 may exist close to the interface between subunits. We recently reported that deletion of the putative juxtamembrane dimer-interface region (aa 560−580) markedly decreased the pH_i-sensitivity of NHE1 (*11*).

The functional significance of oligomerization has only been studied for a few transporters. Some experimental data (*35*−*38*) suggest that NhaA exists as a dimer in membranes and that the subunits may functionally interact. A recent study using a fluorescence resonance energy transfer technique (*38*) suggested that the *Helicobacter pylori* Na^+/H^+ antiporter NhaA monomers exerts conformational change during transport. Furthermore, the transport-deficient mutant form of *Saccaromyces cerevisiae* Na^+/H^+ antiporter Nha1p was reported to exert the dominant-negative effect upon coexpression with the wild-type Nha1p (*39*). These studies suggest the functional importance for dimerization of bacteria and yeast Na^+/H^+ antiporters. The glucose transporter GLUT1 (*40*) and the serotonin transporter SERT (*41*) have also been suggested to function as homo-oligomers, whereas the bacterial lactose permease LacY (*42*) and the renal type IIa Na^+/phosphate cotransporter (*43*) have been shown to function as monomers. However, in the case of NHE1, the functional consequence of dimerization appears to be more complex, that is, dimerization is necessary for NHE1 to function in the physiological pH_i range, although each subunit is capable of functioning at a more acidic pH_i. In this context, it is of interest to note that the lactose transport protein LacS from *Streptococcus thermophilus* was recently shown to be a cooperative dimer in which two subunits are functionally coupled in ΔH^+-driven substrate symport, whereas the monomer is sufficient for substrate/substrate exchange (*44*).

In summary, we presented evidence that dimerization may be essential for NHE1 to exert exchange activity in neutral pH_i range. We predict that two active NHE1 subunits would be required for NHE1 to possess the physiologically relevant H^+ affinity presumably at the H^+-regulatory sites. Although the underlying molecular mechanism is still unknown, our present findings provide good evidence for the functional importance of the dimerization of NHE1.

ACKNOWLEDGMENT

We thank Dr. M. Shigekawa for fruitful discussions and Mrs. M. Nakatani (Ms. M. Ookubo) for technical assistance.

REFERENCES

1. Wakabayashi, S., Shigekawa, M., and Pouyssegur, J. (1997) Molecular physiology of vertebrate Na^+/H^+ exchangers, *Physiol. Rev. 77*, 51−74.
2. Orlowski, J., and Grinstein, S. (2004) Diversity of the mammalian sodium/proton exchanger SLC9 gene family, *Pflugers Arch. 447*, 549−565.
3. Counillon, L., and Pouyssegur, J. (2000) The expanding family of eucaryotic Na^+/H^+ exchangers, *J. Biol. Chem. 275*, 1−4.
4. Putney, L. K., Denker, S. P., and Barber, D. L. (2002) The changing face of the Na^+/H^+ exchanger, NHE1: structure, regulation, and cellular actions, *Annu. Rev. Pharmacol. Toxicol. 42*, 527−552.
5. Slepkov, E., and Fliegel, L. (2002) Structure and function of the NHE1 isoform of the Na^+/H^+ exchanger, *Biochem. Cell Biol. 80*, 499−508.
6. Aronson, P. S., Nee, J., and Suhm, M. A. (1982) Modifier role of internal H^+ in activating the Na^+-H^+ exchanger in renal microvillus membrane vesicles, *Nature 299*, 161−163.
7. Aronson, P. S. (1985) Kinetic properties of the plasma membrane Na^+-H^+ exchanger, *Annu. Rev. Physiol. 47*, 545−560.
8. Wakabayashi, S., Hisamitsu, T., Pang, T., and Shigekawa, M. (2003) Kinetic dissection of two distinct proton binding sites in Na^+/H^+ exchangers by measurement of reverse mode reaction, *J. Biol. Chem. 278*, 43580−43585.
9. Fafournoux, P., Noel, J., and Pouyssegur, J. (1994) Evidence that Na^+/H^+ exchanger isoforms NHE1 and NHE3 exist as stable dimers in membranes with a high degree of specificity for homodimers, *J. Biol. Chem. 269*, 2589−2596.
10. Fliegel, L., Haworth, R. S., and Dyck, J. R. (1993) Characterization of the placental brush border membrane Na^+/H^+ exchanger: identification of thiol-dependent transitions in apparent molecular size, *Biochem. J. 289*, 101−107.
11. Hisamitsu, T., Pang, T., Shigekawa, M., and Wakabayashi, S. (2004) Dimeric interaction between the cytoplasmic domains of the Na^+/H^+ exchanger NHE1 revealed by symmetrical intermolecular cross-linking and selective co-immunoprecipitation, *Biochemistry 43*, 11135−11143.

12. Otsu, K., Kinsella, J., Sacktor, B., and Froehlich, J. P. (1989) Transient state kinetic evidence for an oligomer in the mechanism of Na^+-H^+ exchange, *Proc. Natl. Acad. Sci. U.S.A. 86*, 4818−4822.
13. Otsu, K., Kinsella, J. L., Koh, E., and Froehlich, J. P. (1992) Proton dependence of the partial reactions of the sodium-proton exchanger in renal brush border membranes, *J. Biol. Chem. 267*, 8089−8096.
14. Lacroix, J., Poet, M., Maehrel, C., and Counillon, L. (2004) A mechanism for the activation of the Na/H exchanger NHE-1 by cytoplasmic acidification and mitogens, *EMBO Rep. 5*, 91−96.
15. Bertrand, B., Wakabayashi, S., Ikeda, T., Pouyssegur, J., and Shigekawa, M. (1994) The Na^+/H^+ exchanger isoform 1 (NHE1) is a novel member of the calmodulin-binding proteins. Identification and characterization of calmodulin-binding sites, *J. Biol. Chem. 269*, 13703−13709.
16. Pouyssegur, J., Sardet, C., Franchi, A., L'Allemain, G., and Paris, S. (1984) A specific mutation abolishing Na^+/H^+ antiport activity in hamster fibroblasts precludes growth at neutral and acidic pH, *Proc. Natl. Acad. Sci. U.S.A. 81*, 4833−4837.
17. Wakabayashi, S., Fafournoux, P., Sardet, C., and Pouyssegur, J. (1992) The Na^+/H^+ antiporter cytoplasmic domain mediates growth factor signals and controls "H^+-sensing", *Proc. Natl. Acad. Sci. U.S.A. 89*, 2424−2428.
18. Wakabayashi, S., Pang, T., Su, X., and Shigekawa, M. (2000) A novel topology model of the human Na^+/H^+ exchanger isoform 1, *J. Biol. Chem. 275*, 7942−7949.
19. Ikeda, T., Schmitt, B., Pouyssegur, J., Wakabayashi, S., and Shigekawa, M. (1997) Identification of cytoplasmic subdomains that control pH-sensing of the Na^+/H^+ exchanger (NHE1): pH-maintenance, ATP-sensitive, and flexible loop domains, *J. Biochem. (Tokyo) 121*, 295−303.
20. Huang, Y., Lemieux, M. J., Song, J., Auer, M., and Wang, D. N. (2003) Structure and mechanism of the glycerol-3-phosphate transporter from Escherichia coli, *Science 301*, 616−620.
21. Abramson, J., Smirnova, I., Kasho, V., Verner, G., Kaback, H. R., and Iwata, S. (2003) Structure and mechanism of the lactose permease of Escherichia coli, *Science 301*, 610−615.
22. Lopez-Corcuera, B., Nunez, E., Martinez-Maza, R., Geerlings, A., and Aragon, C. (2001) Substrate-induced conformational changes of extracellular loop 1 in the glycine transporter GLYT2, *J. Biol. Chem. 276*, 43463−43470.
23. Counillon, L., Franchi, A., and Pouyssegur, J. (1993) A point mutation of the Na^+/H^+ exchanger gene (NHE1) and amplification of the mutated allele confer amiloride resistance upon chronic acidosis, *Proc. Natl. Acad. Sci. U.S.A. 90*, 4508−4512.
24. Counillon, L., Noel, J., Reithmeier, R. A., and Pouyssegur, J. (1997) Random mutagenesis reveals a novel site involved in inhibitor interaction within the fourth transmembrane segment of the Na^+/H^+ exchanger-1, *Biochemistry 36*, 2951−2959.
25. Slepkov, E. R., Chow, S., Lemieux, M. J., and Fliegel, L. (2004) Proline residues in transmembrane segment IV are critical for activity, expression and targeting of the Na^+/H^+ exchanger isoform 1, *Biochem. J. 379*, 31−38.
26. Noel, J., Germain, D., and Vadnais, J. (2003) Glutamate 346 of human Na^+-H^+ exchanger NHE1 is crucial for modulating both the affinity for Na^+ and the interaction with amiloride derivatives, *Biochemistry 42*, 15361−15368.
27. Khadilkar, A., Iannuzzi, P., and Orlowski, J. (2001) Identification of sites in the second exomembrane loop and ninth transmembrane helix of the mammalian Na^+/H^+ exchanger important for drug recognition and cation translocation, *J. Biol. Chem. 276*, 43792−43800.
28. Hunte, C., Screpanti, E., Venturi, M., Rimon, A., Padan, E., and Michel, H. (2005) Structure of a Na^+/H^+ antiporter and insights into mechanism of action and regulation by pH, *Nature 435*, 1197−1202.
29. Inoue, H., Noumi, T., Tsuchiya, T., and Kanazawa, H. (1995) Essential aspartic acid residues, Asp-133, Asp-163 and Asp-164, in the transmembrane helices of a Na^+/H^+ antiporter (NhaA) from Escherichia coli, *FEBS Lett. 363*, 264−268.
30. Yamashita, A., Singh, S. K., Kawate, T., Jin, Y., and Gouaux, E. (2005) Crystal structure of a bacterial homologue of Na^+/Cl^--dependent neurotransmitter transporters, *Nature 437*, 215−223.
31. Olkhova, E., Hunte, C., Screpanti, E., Padan, E., and Michel, H. (2006) Multiconformation continuum electrostatics analysis of the NhaA Na^+/H^+ antiporter of Escherichia coli with functional implications, *Proc. Natl. Acad. Sci. U.S.A. 103*, 2629−2634.
32. Wakabayashi, S., Hisamitsu, T., Pang, T., and Shigekawa, M. (2003) Mutations of Arg440 and Gly455/Gly456 oppositely change pH sensing of Na^+/H^+ exchanger 1, *J. Biol. Chem. 278*, 11828−11835.
33. Pang, T., Hisamitsu, T., Mori, H., Shigekawa, M., and Wakabayashi, S. (2004) Role of calcineurin B homologous protein in pH regulation by the Na^+/H^+ exchanger 1: tightly bound Ca^{2+} ions as important structural elements, *Biochemistry 43*, 3628−3636.
34. Pang, T., Su, X., Wakabayashi, S., and Shigekawa, M. (2001) Calcineurin homologous protein as an essential cofactor for Na^+/H^+ exchangers, *J. Biol. Chem. 276*, 17367−17372.
35. Williams, K. A., Geldmacher-Kaufer, U., Padan, E., Schuldiner, S., and Kuhlbrandt, W. (1999) Projection structure of NhaA, a secondary transporter from Escherichia coli, at 4.0 A resolution, *EMBO J. 18*, 3558−3563.
36. Williams, K. A. (2000) Three-dimensional structure of the ion-coupled transport protein NhaA, *Nature 403*, 112−115.
37. Gerchman, Y., Rimon, A., Venturi, M., and Padan, E. (2001) Oligomerization of NhaA, the Na^+/H^+ antiporter of Escherichia coli in the membrane and its functional and structural consequences, *Biochemistry 40*, 3403−3412.
38. Karasawa, A., Tsuboi, Y., Inoue, H., Kinoshita, R., Nakamura, N., and Kanazawa, H. (2005) Detection of oligomerization and conformational changes in the Na^+/H^+ antiporter from Helicobacter pylori by fluorescence resonance energy transfer, *J. Biol. Chem. 280*, 41900−41911.
39. Mitsui, K., Yasui, H., Nakamura, N., and Kanazawa, H. (2005) Oligomerization of the Saccharomyces cerevisiae Na^+/H^+ antiporter Nha1p: implications for its antiporter activity, *Biochim. Biophys. Acta. 1720*, 125−136.
40. Zottola, R. J., Cloherty, E. K., Coderre, P. E., Hansen, A., Hebert, D. N., and Carruthers, A. (1995) Glucose transporter function is controlled by transporter oligomeric structure. A single, intramolecular disulfide promotes GLUT1 tetramerization, *Biochemistry 34*, 9734−9747.
41. Kilic, F., and Rudnick, G. (2000) Oligomerization of serotonin transporter and its functional consequences, *Proc. Natl. Acad. Sci. U.S.A. 97*, 3106−3111.
42. Sahin-Toth, M., Lawrence, M. C., and Kaback, H. R. (1994) Properties of permease dimer, a fusion protein containing two lactose permease molecules from Escherichia coli, *Proc. Natl. Acad. Sci. U.S.A. 91*, 5421−5425.
43. Kohler, K., Forster, I. C., Lambert, G., Biber, J., and Murer, H. (2000) The functional unit of the renal type IIa Na^+/Pi cotransporter is a monomer, *J. Biol. Chem. 275*, 26113−26120.
44. Veenhoff, L. M., Heuberger, E. H., and Poolman, B. (2001) The lactose transport protein is a cooperative dimer with two sugar translocation pathways, *EMBO J. 20*, 3056−3062.

BI0608616

EXPERIMENTAL CELL RESEARCH 312 (2006) 3152-3164

available at www.sciencedirect.com

ScienceDirect

www.elsevier.com/locate/yexcr

Research Article

Identification and characterization of GSRP-56, a novel Golgi-localized spectrin repeat-containing protein

Yuko Kobayashi[a,*], Yuki Katanosaka[a], Yuko Iwata[a], Masayuki Matsuoka[a], Munekazu Shigekawa[b], Shigeo Wakabayashi[a,*]

[a]Department of Molecular Physiology, National Cardiovascular Center Research Institute, Suita, Osaka 565-8565, Japan
[b]Department of Human Life Sciences, Senri Kinran University, Suita, Osaka 565-0873, Japan

ARTICLE INFORMATION

Article Chronology:
Received 30 March 2006
Revised version received
4 June 2006
Accepted 13 June 2006
Available online 27 June 2006

Keywords:
Syne-1
Nesprin-1
Spectrin repeat
Golgi apparatus
Subcellular localization

ABSTRACT

Spectrin repeat (SR)-containing proteins are important for regulation of integrity of biomembranes, not only the plasma membrane but also those of intracellular organelles, such as the Golgi, nucleus, endo/lysosomes, and synaptic vesicles. We identified a novel SR-containing protein, named GSRP-56 (Golgi-localized SR-containing protein-56), by a yeast two-hybrid method, using a member of the transient receptor potential channel family, TRPV2, as bait. GSRP-56 is an isoform derived from a giant SR-containing protein, Syne-1 (synaptic nuclear envelope protein-1, also referred to as Nesprin-1 or Enaptin), predicted to be produced by alternative splicing. Immunological analysis demonstrated that this isoform is a 56-kDa protein, which is localized predominantly in the Golgi apparatus in cardiomyocytes and C2C12 myoblasts/myotubes, and we found that two SR domains were required both for Golgi targeting and for interaction with TRPV2. Interestingly, overexpression of GSRP-56 resulted in a morphological change in the Golgi structure, characterized by its enlargement of cis-Golgi marker antibody-staining area, which would result partly from fragmentation of Golgi membranes. Our findings indicate that GSRP-56 is a novel, particularly small Golgi-localized member of the spectrin family, which possibly play a role in maintenance of the Golgi structure.

© 2006 Elsevier Inc. All rights reserved.

Introduction

The structural integrity of biomembranes, including the plasma membrane, Golgi, nuclear, and endosomal membranes, is maintained by a network formed by multiple organellar-specific cytoskeletal proteins. A protein family containing spectrin repeat (SR) motifs, called the spectrin superfamily, is particularly important for regulation of such membrane stability [1,2]. The SR consists of approximately 106 amino acids, with a characteristic triple-helical bundle comprised of three α-helices connected by two loop regions [3,4]. The SR-containing spectrin superfamily proteins, including spectrin, α-actinin, dystrophin, and utrophin, function as the structural support for most cells by forming linkages of membranes with cytoplasmic structures, and also provide the scaffold for a distinct membrane protein complex [1,5]. Spectrin, a conventional SR-containing protein, was first identified as a protein that lines the plasma

* *Corresponding authors.* Y. Kobayashi is to be contacted at the Department of Human Life Sciences, Senri Kinran University, Suita, Osaka 565-0873, Japan. Fax: +81 6 6872 7872. S. Wakabayashi, fax: +81 6 6835 5314.
E-mail addresses: yu-kobayashi@kinran.ac.jp (Y. Kobayashi), wak@ri.ncvc.go.jp (S. Wakabayashi).

0014-4827/$ - see front matter © 2006 Elsevier Inc. All rights reserved.
doi:10.1016/j.yexcr.2006.06.026

membrane. Some spectrin isoforms are also localized to intracellular organelles other than the plasma membrane, such as the Golgi apparatus, endosome/lysosome, and cytoplasmic vesicles [2,6]. For example, it has been reported that at the Golgi apparatus, β-spectrin isoforms form complexes with Golgi-specific ankyrins and cytoskeletal components, and play roles not only in maintenance of Golgi structure but in vesicular transport of membrane proteins [2,7,8].

Recently, a giant SR-containing protein, Syne-1 (synaptic nuclear envelope protein-1, also referred to as Nesprin-1 or Enaptin) was reported. Syne-1 was identified initially as a binding partner for the acetylcholine receptor in skeletal muscle [9] and then shown to be expressed in multiple forms derived from a very large gene (~500 kb) through transcription at alternative initiation sites and mRNA splicing [10,11]. Among these splicing variants, in addition to the putative longest isoform (Syne-1, 1 MDa), Nesprin-1β and Syne-1B are expressed as protein products of 370–380 kDa with broad tissue distribution, while Nesprin-1α, Syne-1A and myne-1 is muscle-specific proteins of 110–130 kDa [9,10,12]. The longest isoform consists of a N-terminal actin binding domain (ABD), a central multiple SR-containing domain and a C-terminal Klarsicht-related (KASH) transmembrane domain that spans the nuclear membrane, has been suggested to play an important role in nuclear positioning [11,13]. The longest isoform has also been suggested to participate in cytokinesis and vesicular transport via the Golgi [14,15]. The smaller Nesprin-1α, which has an SR-domain and a C-terminal domain, has the ability to bind to nuclear protein lamin A/C and emerin, and was suggested to play roles in bridging the nuclear envelope (NE) [12,16]. Moreover, it has recently been demonstrated that Nesprin-1α can bind to muscle A-kinase anchoring protein (mAKAP) and this molecule has been suggested to act as a receptor for mAKAP on NE [17]. These studies raise the interesting possibility that a diverse array of proteins containing different combinations of SR domains derived from the same giant gene may control various cell functions in a tissue-specific and organellar-specific manner. It is likely that there are many other unidentified forms of SR-containing proteins, which may play crucial roles in cellular functions.

In this study, we identified a novel splicing isoform (named GSRP-56) produced from the gene encoding Syne-1 by a yeast two-hybrid method, using a member of the transient receptor potential channel family, TRPV2 (or growth-factor-regulated channel, GRC) as bait. We identified this potential stretch-activated cation channel, TRPV2, previously as a candidate protein responsible for abnormal Ca^{2+} influx in muscular dystrophy and cardiomyopathy [18]. In this study, we showed that GSRP-56 is a novel Golgi-localized isoform of Syne-1 with an apparent molecular mass of 56 kDa, which is different from the splicing isoforms of Syne-1 reported to date. GSRP-56 contains two SR domains, which are necessary for Golgi localization and for interaction with TRPV2. Overexpression of GSRP-56 in HEK cells resulted in enlargement of the Golgi apparatus. Our data indicate that GSRP-56 is a novel spectrin family member possibly regulating the structural organization of the Golgi apparatus.

Materials and methods

Antibodies and other materials

Commercially available primary antibodies were as follows: mouse monoclonal anti-FLAG M2 (Sigma); mouse monoclonal anti-GAPDH (Chemicon); mouse monoclonal anti-GM130 (Golgin-95); mouse monoclonal anti-TGN38; mouse monoclonal anti-nucleoporin-p62; mouse monoclonal anti-adaptin-γ (BD Biosciences). Antiserum against GSRP-56 was obtained by immunizing a rabbit with the GST fusion protein containing the second SR motif of GSRP-56 (aa 259–358). Rabbit polyclonal anti-TRPV2 was reported previously [18]. Brefeldin A, Phusion DNA polymerase, and competent cells (DH5α) were purchased from Sigma, Finnzymes and TaKaRa, respectively. All other chemicals were of the highest purity available. Protein concentration was determined using a Bicinchoninic acid protein assay kit (Pierce) with bovine serum albumin as a standard. RIPA lysis buffer contains 20 mM HEPES, pH 7.4, 150 mM NaCl, 1% deoxycholate, 0.1% SDS, 0.1% Triton X-100, and protease inhibitors.

Yeast two-hybrid screen and isolation of GSRP-56 cDNA

We used MATCHMAKER3 system (BD Clontech) for the yeast two-hybrid screen. A DNA fragment corresponding to the N-terminal cytosolic region (aa 1–167) of mouse TRPV2 fused to the GAL4 DNA binding domain was used as bait and approximately 2×10^7 clones were screened from a human heart cDNA library fused to the GAL4 activation domain (BD Clontech). The screening procedure was essentially as described previously [19]. Colonies that grew in medium lacking histidine, adenine, leucine, and tryptophan (–HALT) were isolated as positive clones and sequenced. From this screen, we sequenced at least 200 positive clones and finally isolated a partial cDNA encoding GSRP-56. This clone was isolated at high frequency (25 colonies, 12% of positive clones sequenced). A full-length cDNA of GSRP-56 was cloned by an additional screen from a human heart large-insert cDNA library (BD Biosciences) using the C-terminal fragment of GSRP-56 as a probe. Library screening was carried out according to the manufacturer's protocol, and the isolated clone was sequenced in its entirety. The genomic sequence was searched using UCSC BLAT search program [20].

For confirmation of the 5′-upstream structure and the entirety of GSRP-56 mRNA, we designed the following primers: F1 (forward), 5′-TTCTGGGTCCTTGTGGCACA-3′; R1 (reverse), 5′-TTTTACATTCGGGCTTTA-3′. Forward and reverse primers correspond to the direct upstream of putative exon 1 and 3′-UTR region of GSRP-56, respectively (black arrows in Fig. 1B). The GSRP-56 cDNA including 5′-upstream region was isolated by the first PCR amplification using these primers and human heart cDNA (BioChain) as the template, and following nested-PCR amplification using the primers adjacent to the first PCR primers (F2, 5′-GACAGGGTCCCCCTGTGTAC-3′; R2, 5′-CGGGCTTTATTTTATTTT-3′. white arrows in Fig. 1B). Protein sequence motifs were detected using the SMART program [21].